Materials Today Energy 9 (2018) 49–66

Contents lists available at ScienceDirect

Materials Today Energy

journal homepage: www.journals.elsevier.com/materials-today-energy/

# A mini-review on the development of Si-based thin film anodes for Li-ion batteries

Aliya Mukanova [a, b], Albina Jetybayeva [a, b], Seung-Taek Myung [c], Sung-Soo Kim [d], Zhumabay Bakenov [a, b, *]

[a] National Laboratory Astana, School of Engineering, Nazarbayev University, 53 Kabanbay Batyr Av., Astana 010000 Kazakhstan
[b] Institute of Batteries, 53 Kabanbay Batyr Ave., Astana 010000 Kazakhstan
[c] Department of Nano Technology and Advanced Materials Engineering, Sejong University, Gunja-dong, Gwangjin-gu, Seoul, 143-747, Republic of Korea
[d] Graduate School of Energy Science and Technology, Chungnam National University, 99 Daehak Ave., Yuseong-gu, Daejeon, 34134, South Korea

ARTICLE INFO

*Article history:*
Received 15 March 2018
Received in revised form
16 April 2018
Accepted 6 May 2018
Available online 16 May 2018

*Keywords:*
Silicon anode
Silicon-based
Thin film anode
Lithium-ion batteries
Microbatteries

ABSTRACT

This review provides a summary of the progress in research on various Si-based thin films as anode materials for lithium-ion batteries. The lithiation mechanism models, different types of materials from pure monolithic Si thin film to Si-based three-dimensional structured composite thin films, the effect of liquid and solid-state electrolytes on the performance of Si were considered and various available preparation techniques were discussed. A table summarizing important information on such systems including the thin film features, preparation methods and conditions, electrochemical test conditions and obtained results in order to elucidate the approaches used to prepare a stable thin film anode with high capacity and long cycle life is provided. We believe that this review will help the researchers to find some answers and induce some new ideas.



## 1. Introduction

Silicon (Si) has become a forefront candidate among other anode materials suitable for high-performance lithium-ion batteries (LIBs) [1]. The interest of scientists is caused by its high specific capacity of 3579 mAh $g^{-1}$ achievable upon formation of the $Li_{15}Si_4$ silicide, a theoretical volumetric capacity of 2190 mAh $cm^{-3}$, a comparatively low discharge potential of 0.4 V *vs.* $Li/Li^+$, and low cost and safety [2–4]. However, an alloying nature of Si lithiation, which leads to a high capacity, is inevitably accompanied by an undesirable volume expansion. The latter calls a strain stress arising in the Si material bulk that, upon repeated cycling, leads to its mechanical degradation, pulverization, electrical contact loss leading to capacity loss and even to safety issues. There are several silicides like $Li_{12}Si_7$, $Li_7Si_3$, $Li_{13}Si_4$, $Li_{15}Si_4$, $Li_{21}Si_5$, $Li_{17}Si_4$, $Li_{22}Si_5$ which can be formed depending on conditions. In this review paper, we consider $Li_{15}Si_4$ as the highest lithiated phase, which forms below the potential of 50 mV at room temperature [5], because the silicides with the higher lithiation form usually at the temperatures above 100 °C [6].

Amorphous and crystalline Si (a-Si and c-Si, respectively) can be both used as anode materials. However, a crystalline structure has been reported to be inactive until becoming amorphous after the first alloying with lithium ($Li^+$) ions. One of the first clarifying works on this was carried out by Obrovac et al. [5] who investigated c-Si using XRD and observed its conversion to partially lithiated a-Si during the first discharge, following by a-Si suddenly crystallized into $Li_{15}Si_4$ below 50 mV, which is a fully lithiated phase at room temperature. This phase is associated with high internal stresses with particle cracking, poor electrical contact, and capacity fading. The authors suggested restricting cycling in the potential ranges above 50 mV. Research group of Graetz et al. [7] studied the a-Si film and nanocrystalline Si film, where a-Si showed a higher initial reversible specific capacity of 2500 mAh $g^{-1}$, meanwhile, nanocrystalline Si exhibited a reversible capacity of 1000 mAh $g^{-1}$ that was explained by the fact that c-Si has a slow activation rate via the transformation of material from crystalline to amorphous phase. In addition, c-Si provides fewer pathways for $Li^+$ ions insertion, possesses nonuniform expansion in contrast with a-Si. Therefore, the

* Corresponding author. National Laboratory Astana, School of Engineering, Nazarbayev University, Institute of Batteries, 53 Kabanbay Batyr Av., Astana 010000 Kazakhstan.
*E-mail address:* zbakenov@nu.edu.kz (Z. Bakenov).

https://doi.org/10.1016/j.mtener.2018.05.004
2468-6069/

amorphous phase of Si is able to provide higher specific capacity and longer cycle life than c-Si [8–11].

Moving from macro-to nanoscale structures can result in a significant improvement of electrochemical characteristics of the Si-based anodes for the next-generation LIBs. Many researcher teams have shown that nanosized Si particles are exposed to less degradation due to high surface energy as well as more active sites due to the high surface area [12]. It is known that one of the significant drawbacks of Si anode is a thick solid electrolyte interface (SEI), which usually forms upon its first lithiation on its surface, and impedes $Li^+$ ions insertion/extraction and delays electrochemical reaction resulting in the reduction of capacity [10]. In case of nanoscale Si, the high surface area leads to an increased irreversible capacity in the few first cycles. This arises due trapping $Li^+$ ions into the SEI during its intensive formation. Indeed, this fact should be taken into account when working on improving the performance of Si anodes [13]. The immense efforts have been done to improve the capacity retention using various strategies [10,14]. Thin film Si anode is one of the most promising nanostructured materials of great interest for next-generation Li-ion microbattery (LIMBs) technologies, which is inherently simple in concept and comprising fire-safe solid state components of lightweight and compact configuration [15,16]. The advantages of thin films are the lower expansion at the nanoscale, the better electrical conductivity of dense thin film, and absence of binders. Besides, the Si thin film can be deposited directly on any shape with any size using the same techniques as for microdevices manufacturing. The thickness of such batteries may range within 15 μm, which allows achieving high volumetric energy densities. LIMBs have been intensively developed to power a diverse range of applications, such as neural and cardio simulators, smart cards, drug delivery systems, small-scale sensors and security devices, radio frequency identification devices, actuators, eye lenses, and many other portable microelectronics [9,17].

During the recent two decades, a growing number of research works have been devoted to design Si thin film anode for the emerging and future applications [18,19]; however, the problems with volume variation and accompanied rapid capacity fading still demand a practical solution to satisfy the requirements for such materials. Various techniques have been used to deposit Si such as electrodeposition, chemical vapor deposition (CVD), vacuum evaporation (VE), electron beam evaporation (EBE), ballistic consolidation (BC), magnetron sputtering (MS), glow discharge plasma deposition (GDPD), pulsed laser deposition (PLD) etc. Si thin film performance was investigated in terms of its dependence on various properties such as phase state (amorphous, crystalline), film thickness, substrate surface condition, Si microstructure and composition, doping, voltage range, electrolyte type and its composition, etc. In the present review, we realized an attempt to collect the results available up to date, to systematize them based on the deposition methods.

To our knowledge, this is the first review with the main focus on the development of Si-based thin film anode for LIBs which accurately systematizes the existing knowledge on the understanding the Si film anode lithiation/delithiation reactions and degradation mechanisms, describes the possible solutions for the improvement of cycling performance as well as provides the table with the most informative details on Si thin film anode.

## 2. Lithiation mechanism and stresses

In general, the lithiation process of Si thin films investigated by conventional electrochemical testing methods and advanced in-situ optical and structural techniques is similar to that determined for other Si materials. The electrochemical reactions in such cell start from the SEI formation on the surface of Si film that usually occurs around 0.4–0.5 V *vs.* $Li/Li^+$ at the first lithiation stage. An alloying mechanism in Si thin films has been found to have a step-by-step behavior: lithiation reaction onset with LiSi formation at a potential of ~0.4 V and further lithiation with formation of $Li_{1.7}Si$ at 0.3 V, $Li_{3.25}Si$ at around 0.2 V, and $Li_xSi$ ($x = 3.75$, 4.2, 4.4) at the potentials below 0.1 V [9,20–25]. However, lithiation of different regions in Si thin films occurs differently. Fig. 1 shows a highly lithiated phase between Si and Cu current collector, non-lithiated Si regions, and fast-diffusion paths filled by $Li^+$ formed at the beginning of the lithiation process induced by Si deposition defects. Supposedly, $Li^+$ insertion can be originated from two sides: from an electrolyte and from a fast diffusion path in a direction parallel to the current collector [23]. Further, in the review, the lithiation process is also referred as happening upon discharge for Si–Li half-cells, while the delithiation corresponds to the charge stage.

The apparent diffusion coefficients ($D$) of $Li^+$ ions in Si thin films, evaluated by several researchers, are summarized in Table 1. According to these data [26–28], it can be supposed that the diffusion coefficient increases with the thickness of the film. Besides, it was found that the effect of ionic diffusivity on the cell performance is insignificant at low C-rates and becomes remarkable at higher current densities ($C > 0.1$). So that, the capacity of the electrode drops faster for low diffusion coefficients rather than for the high ones. Moreover, the effect of standard rate constant was also investigated and, in this case, low diffusion coefficient values resulted in the adverse effect on the capacities even at low C-rates [29]. $Li^+$ ion permeation through thin $Li_xSi$ layers in a multilayer structure between isotopically modulated $LiNbO_3$ layers, serving as tracer reservoirs, was investigated using neutron reflectometry with rapid thermal annealing instruments. It was found that $Li^+$ ions permeability with $x = 0.1$ at 255 °C is $P = (3.3 \pm 0.9) \cdot 10^{-21}$ $m^2$ $s^{-1}$, which is identical to that for pure a-Si. Authors suggested that diffusion more likely occurs in pure a-Si domains rather than along Li–Si-rich percolation paths [30].

The stresses in thin film accompanying lithiation are going through sequential steps depending on the $Li_xSi$ alloy: slight increase of compressive stress (0.3 V), high stresses (0.3–0.1 V) and large stresses because of a three-four times volume expansion at potentials around 0 V [33]. A multi-scale model developed to predict the electrochemical and mechanical behavior of Si showed that the compressive stress induced by the volumetric strain enlarges the migration energy barrier, thus causing accumulation of $Li^+$ ions near the thin film surface, which results in a potential drop. Though, with further lithiation, the mixing enthalpy increases the chemical potential leading to uniform $Li^+$ ions concentration profile [34].

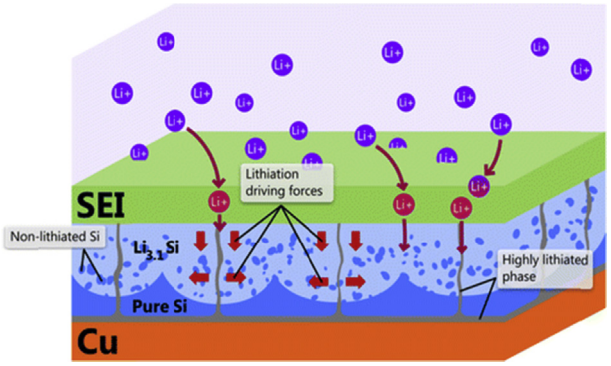


**Fig. 1.** Schematic view of lithiation mechanism in Si thin film [23]. Copyright (2015) American Chemical Society.

**Table 1**
Summary of $Li^+$ ions diffusion coefficients for Si thin films.

| Name | Thickness, nm | Diffusion coefficient, $D$, $cm^2/s$ | Ref. |
|---|---|---|---|
| Undoped Si (CVD) | 50–14 000 | $10^{-10} - 10^{-13}$ | [26] |
| n-type a-Si (MS) | 275 | $(1.47–2.16)\cdot10^{-9}$ | [25] |
| a-Si:H (GD) | 250–700 | $4\cdot10^{-9} - 10^{-13}$ | [27,28] |
| a-Si (PLD) | 120 | $10^{-13}$ | [31] |
| Fullerene coated Si | NA | $\sim 4 \times 10^{-9}$ | [32] |

Other attempts to simulate mechanical behavior of Si thin film during $Li^+$ ions insertion and extraction showed that the stresses in film and substrate due to a huge volume changes of Si play a crucial role in mechanical fracture and delamination of Si film leading to the electrode failure [35–38]. The analysis of relative volume changes for lithiation of 40 and 140 nm a-Si thin films made by in–operando neutron reflectometry revealed a linear volume increase as a function of lithiation time and Li content independent of current density and initial film thickness [39]. Besides, it was observed that the higher capacity loss happens as the thickness of Si films decreases. This is due to the fact that a thinner film easier traps $Li^+$ ions in its bulk and at the interfaces, and leads to higher volume changes [40]. In general, the thickness of SEI, formed during the first cycle, does not depend directly on the Si film thickness; however, it may contribute more significantly on the irreversible capacity as well as the volume change when very thin Si films used [40,41]. For example, in case of a 100 nm thick Si film electrode the formation of SEI may contribute up to 60% of the electrode volume changes. Along with this, an increase of SEI layer, together with Li atoms trapping in the electrode bulk, can result in limited $Li^+$ ionic transport [42]. On the other hand, Tokranov et al. showed that the morphology of SEI on Si film electrode can be affected by conditions during the first lithiation cycle [43]. A soft SEI layer can be produced over a long period of time at higher potentials, whereas harder inorganic phases form at lower potentials. Also, it was reported, that the resistance of the SEI layer reduced upon the initial 20 cycles.

## 3. Silicon thin film anodes

### 3.1. Pure silicon thin films

Bourderau et al. made the first steps in developing Si thin film anodes for LIBs [8], though, their initial results demonstrated a poor performance of anode with only 20% capacity retention after 20 cycles. It was observed later that the decrease of the lower cutting off potential to 0.1 V [33] or even to 0.2 V [43,44] can significantly affect the capacity retention of a-Si thin film improving its cycling performance due to the prevention of high-stage lithiation and the emergence of high stress during the material expansion. However, at the same time, the practical capacity that can be delivered at chosen potential range constituted only 400 mAh $g^{-1}$ during 400 cycles [43,44].

The first deep research of Si thin film was done by Maranchi et al. [9]. Reprinted Fig. 2 shows a cross-section view of as-deposited thin film and its SEM top image after cycling. The authors reported on a dependency of cyclability and reversible capacity on the film thickness as well. Significant degradation of the a-Si thin film was observed by SEM (see Fig. 2b). The separated islands of material appeared after the 1st cycle and the gaps between them tended to expand with time. Formation of these islands was supposedly caused by plastic deformation of the Cu foil serving as a substrate. Electrochemical volume expansion/contraction induced incremental plastic strain (ratcheting) results in widening gaps between the islands during cycling. Delamination of a compressively stressed film on Cu has resulted from the interface imperfection. TEM and EDX analysis showed that atomic intermixing has occurred between the film and substrate, with the interfacial region expanding from 26 nm (as-deposited) to 275 nm (after 30 cycles). The possible nucleation of a lithium copper silicide ($Cu_2LiSi$) crystalline phase weakened the interfacial regions between Si and Cu, leading to the loss of electrical contact [45].

The regularity that the decrease of Si thin film electrode thickness positively affects its cyclability has been observed later in numerous experimental works and confirmed by computational works as well [28,46–50]. The best performance was reported by Ohara et al. for the 50 nm thick Si film that retained a specific capacity of around 3100 mAh $g^{-1}$ after 1000 cycles at 12 C rate with the coulombic efficiency of 100% [51–53].

In addition, in the same work, the effect of doping (intrinsic, p-type and n-type) has been investigated, where the n-type doped Si showed the better electrochemical performance due to enhanced electrical conductivity and reduced charge transfer resistance on the surface of the doped Si electrodes [54]. However, the performance deteriorates when moving from half-cell to full-cell configuration tests. For example, the n-type doped 100 nm a-Si thin film and lithium cobalt oxide ($LiCoO_2$) cathode exhibited only around 60% of the initial reversible capacity at the 30$^{th}$ cycle (~1100 mAh $g^{-1}$) [55]. Another full cell test with a 330 nm thick a-Si thin film and carbon(C)-coated lithium iron phosphate ($LiFePO_4$) cathode delivered a delithiation capacity of only 120 mAh $g^{-1}$ at the 100$^{th}$ cycle [56].

Modification of substrate surface prior to Si film deposition was found to be crucial for attaining a prolonged cycling stability. Roughening of Cu foil with sandpaper in order to expand the contact area with deposited a-Si film, helped the film to accommodate the volume changes [57,58]. Etching a substrate in iron trichloride ($FeCl_3$) was proposed with the same goal and showed the capacity improvement even for the thicker Si thin films (1 μm, 3.6 μm) [53,59]. Another original route – a treatment of a substrate by plasma immersion lanthanum ion implantation, afforded Si thin film anode to achieve a capacity retention of 93% at the 80$^{th}$ cycle [47]. Electrodepositing, used to obtain the rough surface Cu foil, was intended to improve the performance of a 6 μm n-type doped a-Si, however, the anode demonstrated a capacity retention of only 42% after the 1st discharge [60]. Annealing the as-prepared anodes at 300 °C prior to the cell assembly was also to be reported to improve an adhesion strength between Si and Cu, and, consequently, to achieve better electrochemical performance [25].

Another successful strategy to overcome the material degradation from a repetitive volume changes were offered via the design of the density modulated multilayer p-type doped a-Si thin film anodes (see Fig. 3). The low dense layers served as a buffer of expansion between the high dense layers preventing the crack propagation in the film [61,62].

The simulation works, performed with the use of a modified spring-block model, have determined that prevention of capacity fading due to the crack formation during lithiation/delithiation can be achieved by optimization of characteristic size of the thin film and average cracked area (island surface area). Two routes can be employed to design the stable anode: patterning electrode with the pattern size smaller than the average cracked size for a specific film thickness and mentioned above reduction of a film thickness to less than the critical thicknesses (depending on a thickness of the current collector) [50]. Various patterns and structures were employed to improve electrochemical properties of the anode. The lozenge-shaped tiles (Fig. 4a–c), which was obtained by masking a substrate during deposition, allowed to retain up to 91% of capacity after 100 cycles owing to the excellent stress suppression effect during lithiation/delithiation due to

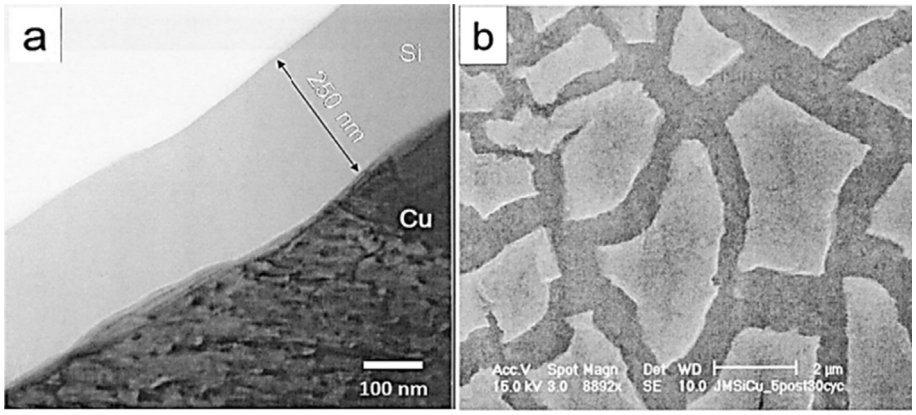


**Fig. 2.** (a) Cross-sectional TEM bright field image of as-deposited 250 nm Si film on Cu. (b) SEM morphology of Si film on Cu after 30$^{th}$ cycles at a C/2.5 rate [9]. Copyright (2003) The Electrochemical Society.

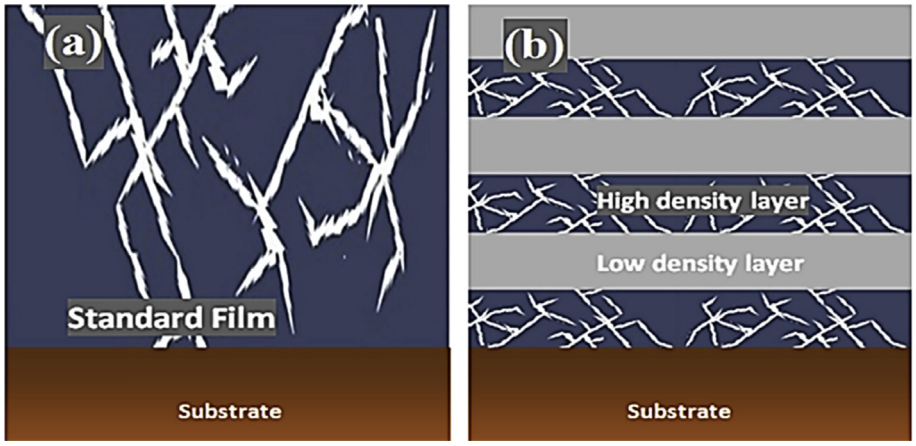


**Fig. 3.** Demonstration of crack propagation in (a) standard high density Si thin films and (b) density modulated multilayer Si thin films [61]. Copyright (2015) Elsevier.

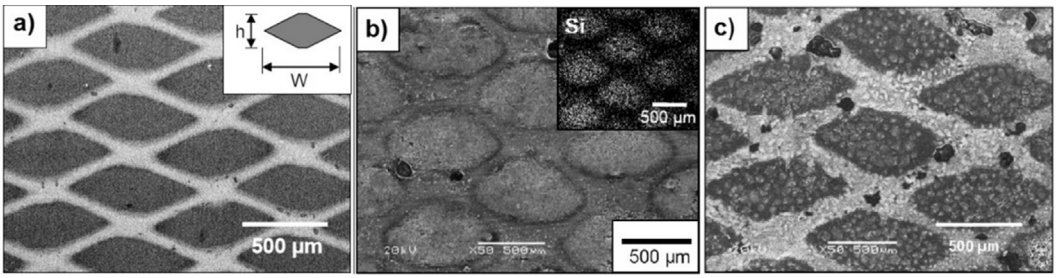


**Fig. 4.** SEM images of Si thin film with lozenge-patterned holes (a) flat before cycling and (b) flat after 10 cycles [63], (c) rough after 50 cycles [64]. Copyright (2012) Springer and Elsevier.

the spaces between Si tiles (Fig. 5), good adhesion and enhanced mechanical stability of the patterned Si thin film anode [63,64]. Besides, the decrease of pattern's size (7–10 μm) showed the higher structural stability of the film without its delamination from substrate [65]. The design of the anode with the trenches prepared by etching an ink-coated Cu foil and covered by Si thin film (Fig. 6), also resulted in the improvement of electrochemical performance and achieving 60% capacity retention after 100 cycles [66,67]. Fig. 7a and b illustrates externally similar structure to the previous, but different in its concept. Here, the anode system with Si ribbons on the soft elastomeric substrate (poly(-dimethylsiloxane), PDMS) had a stretchable nature that helped to levitate a strain stress in Si during the volume changes at $Li^+$ ions extraction/insertion [68].

Investigation and comparison of the planar and shaped Si nanostructures clearly demonstrated the priority of a three dimensional (3D) structured electrode, which is able to achieve high surface area, increase current density and improve a mechanical stability. For example, the low densely packed nanopillars, prepared from the n-type monolithic doped a-Si by etching, showed an excellent cycling performance during 50 cycles with almost no capacity loss [49]. Another 3D shape, a honeycomb-structure of an n-type doped a-Si (Fig. 8a), was designed using lithography technique for etching. Fig. 8b shows the recorded

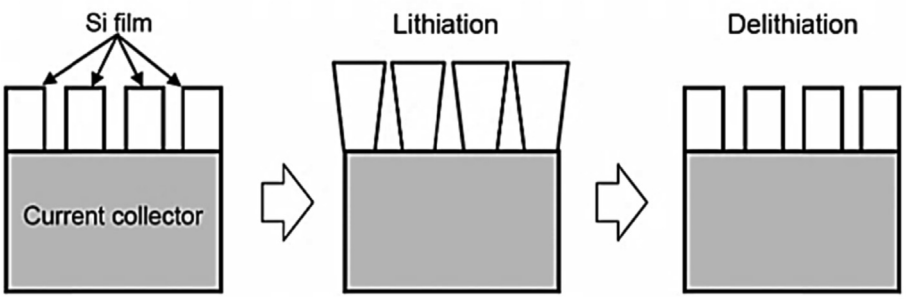


**Fig. 5.** Schematic diagrams of the structural change in patterned Si film electrodes during the charge-discharge (lithiation/delithiation) process [63]. Copyright (2012) Springer.

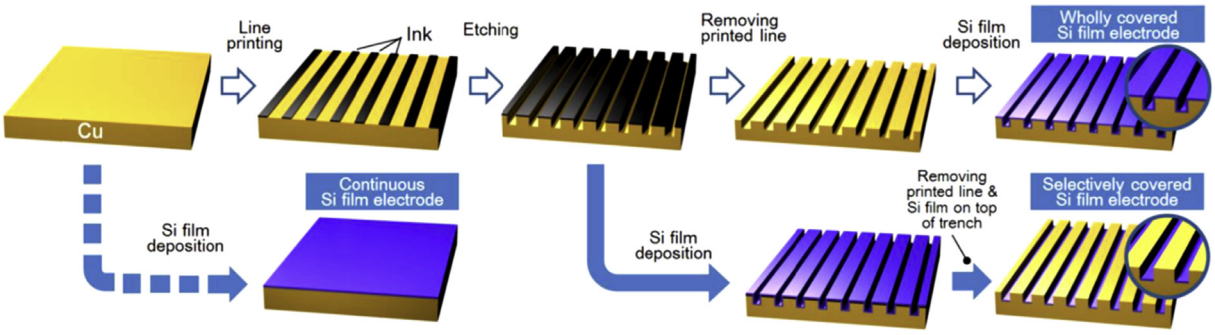


**Fig. 6.** The surface morphology of continuous, wholly covered Si thin film electrode and selectively covered Si thin film electrode [66]. Copyright (2012) Elsevier.

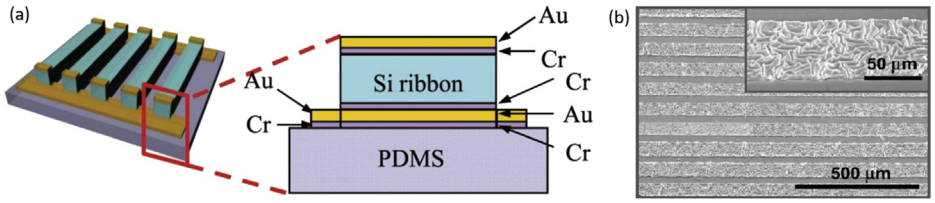


**Fig. 7.** (a) Si anode on poly(dimethylsiloxane) PDMS substrate, (b) SEM images show the buckled Si after lithiation, after six charge/discharge cycles at 1 C [68]. Copyright (2012) Willey.

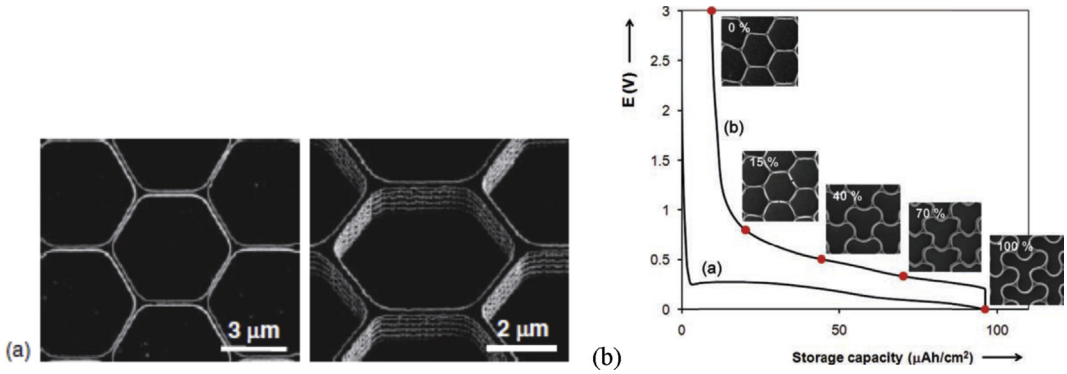


**Fig. 8.** (a) SEM top and tilted view photographs of as-prepared Si honeycombs. (b) Morphological changes of the Si honeycomb structure [69]. Copyright (2011) Willey.

voltage profile of this anode with the inserts of SEM images corresponding to various lithiation contents (in %). Mechanical deformation of honeycomb walls resulted from the occurring internal stress during lithiation and tended to gradual conversion back during delithiation to the nearly original hexagonal structure upon 50 cycles [69]. The Si nanowires perform superior electrochemical properties and long cycle life attributed to the high porosity and electron conductivity of the anode [70–72]. Mathematical model simulation confirmed that the porosity and larger pore size provide a stabilized structure during charge/discharge process [72].

The use of a 3D structured substrate for thin film deposition was demonstrated as one of the most effective ways to achieve the stability in Si anode cycling. A strengthened conductive framework, made from synthesized Cu nanowires with enhanced electrical

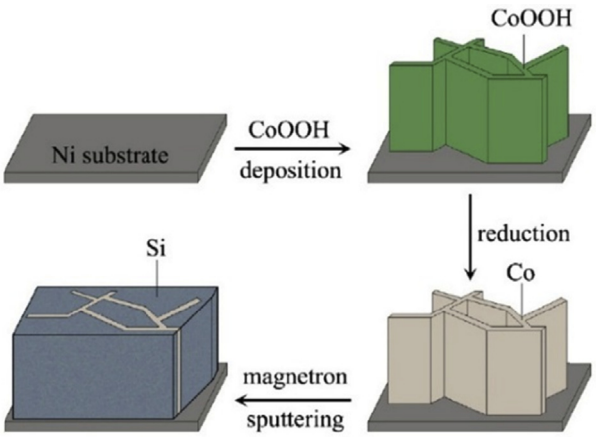


**Fig. 9.** Schematic diagram of the preparation process of cobalt nanosheet arrays supported Si film [76]. Copyright (2016) Elsevier.

connection by 'tight-contact' deposition was used as a substrate for a-Si film. The capacity retention constituted around 90% after 60 cycles [73]. A porous Cu foil prepared by etching in ammonia solution and employed as a current collector for a 400 nm thick a-Si thin film could significantly improve the capacity retention in the comparison with flat and rough substrates [74]. Si thin film, deposited on a Cu foam [75] resulted in a high mass loading of the active material (Si) and a very good cycling stability. The interconnected conductive network facilitated charge transfer in the Si film and avoided the severe pulverization and cracking due to the volume changes. Another 3D current collector – a cobalt nanosheet arrays (Fig. 9), helped to hold 82% of the initial reversible capacity delivered by Si thin film over 100 cycles [76].

Fig. 10a and b show SEM top-view of the Si anode on Tobacco mosaic virus (Si/TMV) covered by nickel, and TEM image of a single Si coated conductive nanowire, respectively [77]. In order to reduce the first cycle irreversible capacity, annealing of the prepared anode was carried out at 350 °C that allowed decreasing the initial irreversible capacity up to 42.6%. In addition, Si was coated by polyacrylonitrile (PAN) followed by its carbonization at 500 °C in Ar, this helped to improve the irreversible capacity up to 22.5%. The 3D Si electrode demonstrated a reversible capacity of 2300 mAh $g^{-1}$ and a capacity of 1200 mAh $g^{-1}$ at the 173$^{rd}$ cycle. In spite of the capacity fading, the 3D patterned Si film electrode showed a good rate capability with a capacity decrease from 1818 to 985 mAh $g^{-1}$ upon the C-rate increase from 0.25 C to 4 C [77].

### 3.2. Silicon-based thin film composites and alloys

Considering the above, the development of Si-based composites and alloys could be a predictable approach towards a stable electrode with a specific capacity higher than that of conventional graphite anode. Similar to a micro-scale powder-based electrode technology, a mixture of materials can be easily employed at the nanoscale as well. For the past decade, there were studies on the combinations of active Si with various components like Cu [78–80], Mo [81], Fe [82,83], Al [84], B [85], Y [86], Ti [87], etc., as well as electrochemically active carbon nanomaterials.

The formation of metal silicide (Si–Mo, Si–Cu, Si–B, Si–Ti) film was reported to reduce electrical resistance and improve mechanical properties of the system due to the existence of additional chemical bonding [78–81,85,88,89]. Coatings such as Cu [90], $Cu_2O$ [91], C [92–95], silicon nitride (SiN) [96] on the surface of Si thin film are used as a protecting top layer, which provides mechanical stability, forms a stable SEI in contact with an electrolyte. In order to provide conditions for $Li^+$ ions diffusion, the coatings have to be very thin and porous. Thus, the properly deposited coating may improve surface electronic conductivity and suppress the electrical contact loss. For example, a-Si thin film with carbon coating, containing some amount of Cu particles (Fig. 11), did not show any damaging after 1000 cycles [95]. Si thin film coated with a 100 nm layer of fullerene showed a remarkable improvement in the electrochemical impedance of thin film [94]. SiN-coated Si anode demonstrated enhanced electrochemical performance with higher capacity due to the formation of a $Li_3N$ film, which resulted in an increased ionic conductivity. The low charge transfer resistance in such layers allowed for cycling at high rates up to 10 C. Besides, the thinner layer of $SiN_x$ is observed to be more effective since the inert nature of SiN might prevent $Li^+$ ions transport and reduce the capacity [96].

Multilayer structured anode with Si thin film and Fe [82,83], Al [84], Y [86], Ti [87], Ta [97], C [29,92,93,98] interlayers, which can act as a conductive component as well as a mechanical buffer during volume changes, illustrated an enhanced cycle life of the electrode. In contrast with planar multilayered electrodes, a 3D nanostructured Si–Al multilayer film (Fig. 12) [84], a 3D Si–Cu–Ti thin film with $Cu_3Si$ nanowires [99], and Si on $TiO_2$ nanotubes [100] could effectively accommodate the volume changes and improve

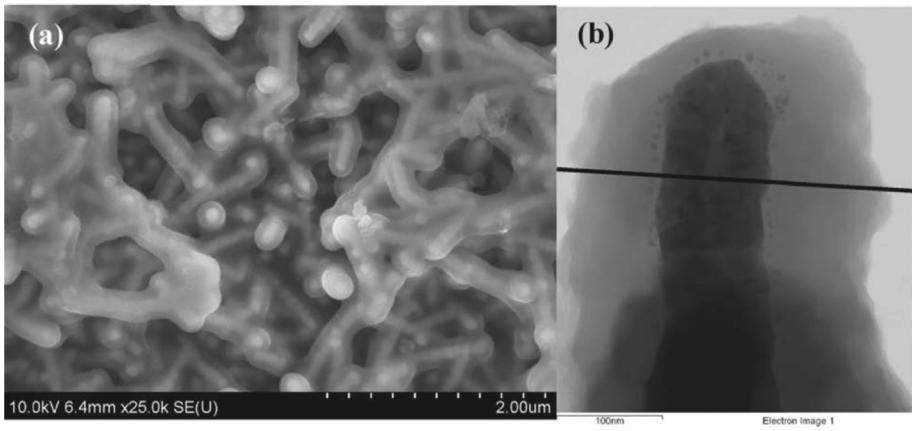


**Fig. 10.** (a) SEM image of 3D Si anode and (b) TEM image of a single nickel-Si core-shell nanowire [77]. Copyright (2011) Willey.

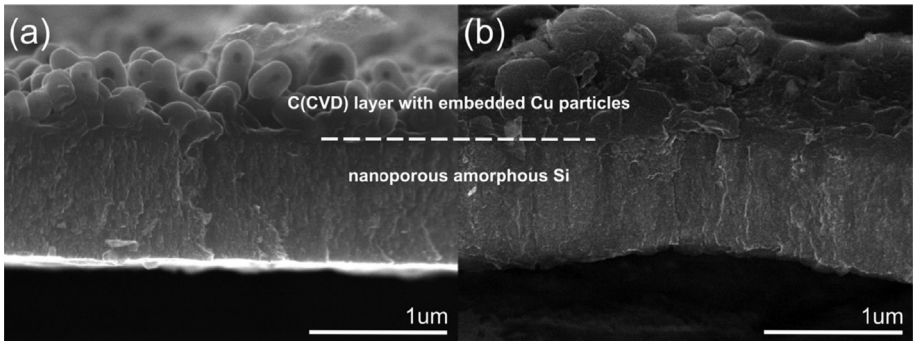


**Fig. 11.** SEM image of sample Si + C (a) before and (b) after cycling [95]. Copyright (2015) Elsevier.

electronic conductivity of the anode, enhancing its electrochemical performance. Multilayered Au–Ti/Si/LIPON/$SnO_2$ anode prepared by sputtering demonstrated a slightly alternating capacity, however, with no visible capacity loss during 200 cycles. This was explained by a LiPON/$SnO_2$ layer acting as a stable porous SEI layer [101]. The challenge for multilayered Si-based thin film anodes is that the thickness, density and amount of layers should be optimized accurately to provide enough mass of active Si and a positive influence on $Li^+$ ion diffusion kinetics and coulombic efficiency.

Similar to conventional Si/C-based composite anodes for LIBs [102], incorporation of carbon materials into Si thin film is a widespread concept to prepare high-performance electrode [32,94,103–107]. Taking into account that C materials can be intercalated by $Li^+$ ions, they can contribute to the total capacity of the thin film electrode significantly. Graphene and carbon nanotubes (CNT) can reach the capacity as high as two times more than conventional graphite [108–110]. Moreover, pure graphene-based anodes were reported to achieve a capacity up to 1116 mAh $g^{-1}$ when lithium ions occupy the adjacent sites of graphene sheets and where $LiC_2$ intercalates form [110]. In addition, the SEI layer on carbon nanomaterial is more stable compared that at pure Si, and, therefore, the combination of Si and C can benefit and provide high capacity and energy [111,112]. For example, a multilayer graphene deposited on the nickel foam, acting as a substrate for Si thin film, displayed a stable capacity of ~2400 mAh $g^{-1}$ with a capacity retention of 75% after 45 cycles [107]. The effect of graphene on the stability improvement was observed due to the enhanced adhesion at the Si-graphene interface [104,106,107].

### 3.3. A notice on the capacity calculations

Indeed, the accurate estimation of Si active mass in a thin film is a key moment for the correct calculation of achieved capacity. It was noticed in a process of this review preparation, that in most cases the mass of active Si was obtained via the volume-density equation. However, there is a risk to obtain the errors related to nonuniformity of film thickness over a substrate. On the other hand, the use of a standard Si density (2.33 g $cm^{-3}$) also causes an error since this value is correct for c-Si only. In fact, the density for a-Si is much lower than that for c-Si and may vary depending on deposition conditions [113]. In order to avoid these challenges and obtain precise results for the Si weight, the Sauerbrey equation could be applied using the frequency values recorded by quartz crystal microbalance (QCM) [61]. Other possible advanced techniques for direct measurements of density are X-ray reflectometry or nanoindentation characterization techniques.

In the recently reported works, the areal capacity is most often represented in [μAh $cm^{-2}$] and the volumetric capacity is in [μAh $cm^{-2}$ μm], where the latter one is more informative and provide an opportunity to easily compare the data.

## 4. Electrolytes for Si thin film anodes

### 4.1. Liquid electrolytes

SEI layer formation plays a key role in cycling stability of the Si electrode. The morphology of the SEI layer is important for long

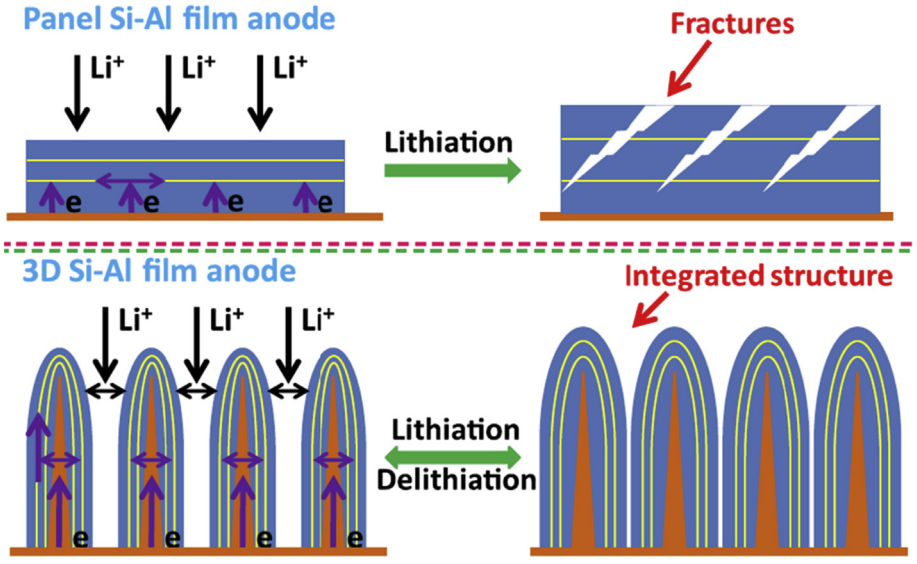


**Fig. 12.** Schematic illustration of mechanism of 3D Si–Al electrode operation with improvement in its electrochemical performance [84]. Copyright (2016) Elsevier.

cycle life and can be dependent on anode surface conditions, and especially on the Si particle size. In case of remarkable expansion of micro-sized Si particles, the extensive fractures are observed on the SEI layer surface. These fractures overgrow with the newly occurring electrolyte decomposition on the Si surface, forming a 'scar tissue' like structure which delays the $Li^+$ ion transport into the anode resulting in capacity decrease [10,114]. On the other hand, the uncontrollable growth of SEI layer uses up high amounts of $Li^+$ ions and electrolyte and leads to an increase in the cell resistance, thus resulting in a capacity fade and an unstable electrochemical performance [115]. The initial capacity loss is significantly affected by the initial content of oxygen on the film surface. The oxides extensively react with $Li^+$ ions in a liquid electrolyte with the irreversible formation of $Li_2O$. Removing the oxides before battery assembling decreases the irreversible capacity as well as enhances the electrode cycling stability [49].

SEI layer on Si is usually a compound of several chemical components emerging during liquid electrolyte decomposition on the Si-based electrode surface. Fig. 13a and b shows the molecular composition of the SEI layer forming in case of a liquid electrolyte 1 M lithium hexafluorophosphate ($LPF_6$) in ethylene carbonate (EC): diethyl carbonate (DC) (1:1, v/v) at the various charged and discharged states determined by high-resolution XPS analysis. It can be seen from Fig. 13a that Si signal disappears at the first charge around 0.1 V, meaning the SEI layer thickness becomes thicker than the XPS penetration depth (~10 nm). In course of time, Li carbonate tends to prevail as the amount of the rest products decreases [116].

The comparison of two electrolytes, lithium bis(oxalato) borate (LiBOB) and $LiPF_6$ electrolytes in the same mixed solvent EC: DC (3:7, v/v) showed a remarkable improvement of discharge capacity retention in case of the first electrolyte. This was ascribed to the formation of the SEI layer with a less-porous structure. The use of 1 M LiBOB electrolyte enabled increasing the conductivity of the a-Si electrode by approximately 3.5 orders of magnitude, which attributed to the formation of LiSi alloy, possessing metallic properties [117]. The investigation of additive-free 1 M lithium bis(trifluoromethylsulphonyl)imide (LiTFSI) in N-methyl, N-propylpiperidinium bis(trifluoromethanesulfonyl)imide (MPPpTFSI) electrolyte showed that the high anodic stability of this ionic liquid may help to develop a very high energy density system [55].

The carbonate additives like fluoroethylene carbonate (FEC), vinylene carbonate (VC) and propylene carbonate (PC) were reported to improve the SEI layer morphology. Choi et al. demonstrated the ability of FEC additive (3%) introduced into 1.3 M $LiPF_6$ in EC: DC (3:7, v/v) electrolyte to improve SEI layer structure. The formation of more smooth and stable SEI facilitated $Li^+$ ions drift to material and led to an increase of the capacity retention by 20.6% in the final 80$^{th}$ cycle [118]. Similarly, the effect of FEC additive in 1 M $LiPF_6$ in FEC: dimethyl carbonate (DMC) (1:4, v/v) was studied in the full $Li^+$ ion cell composed of a-Si thin film anode and a high voltage lithium nickel manganese oxide ($LiNi_{0.5}Mn_{1.5}O_4$) spinel composite cathode. It was found that FEC promoted a full cell to have the capacity retention of 74.2% after 500 cycles. The improved performance was attributed to the good passivation of the Si anode surface and effective passivation of the surface of the high voltage cathode [119]. It was reported that FEC may remarkably improve the long-term cycle performance of Si-based electrodes [55,90,116].

1% VC added into the electrolyte was also observed to assist in the formation of a smooth and uniform SEI layer on Si film, resulting in a 97% of initial capacity value in the 200$^{th}$ cycle retained by a 150 nm thick n-type doped Si thin film [120]. In another research, a combination of 2% VC and 10% FEC in 1 M $LiPF_6$ in EC: DC: ethyl methyl carbonate (EMC) (1:1:1, v/v/v) exhibited an improved capacity retention [84]. The electrochemical performance of 1 M lithium perchlorate ($LiClO_4$) in PC solvent was compared with the same electrolyte in a mixture of EC: DMC (1:1, v/v), where finally both solvents were found to have identical influence. However, it was recommended to use PC additive due to its low cost and an ability to work at low temperatures [51]. Besides, the effect of the electrolyte composition on the irreversible capacity of Si electrodes, particularly in PC-based and EC:DC-based electrolytes, did not reveal a significant difference between them [121].

The effects of trimethoxymethyl silane (TMOS, $CH_3Si[OCH_3]_3$) additive (in 1 M $LiPF_6$ in EC: DC (1:1, v/v) electrolyte) on SEI layer formation was studied for c-Si thin film electrode. It was detected that TMOS can effectively protect the Si surface, producing a stable SEI layer composed of organics with alkyl carbonate and carboxylic acid metal salt functionalities, and phosphorus and fluorine (PF) containing species, leading to a stable cycling at 0.1–1.5 V vs. $Li/Li^+$ delivering 2400 mAh $g^{-1}$ over 200 cycles. The authors reported that PF-containing species, obtained on the Si film surface after cycling without using TMOS, were responsible for the inefficient passivation of the Si surface, resulting in a rapid capacity fade [122].

Another study by Ryu et al. [123] investigated the effect of alkoxysilane additives in lithium battery electrolyte. A significant overpotential growth and an aggravating capacity for discharge/charge process were attributed to the sedimentation of the product of the electrolyte reduction. Moreover, the additives of alkoxysilane acted as a passivation agent for Li cells with Si anode. In general, the presence of such additives prevented a massive accumulation of irreversible electrolyte reduction products on the Si electrode, thus improving the electrode's cycle life.

The gas evolution usually occurs upon decomposition of the components of liquid electrolyte during the lithiation/delithiation

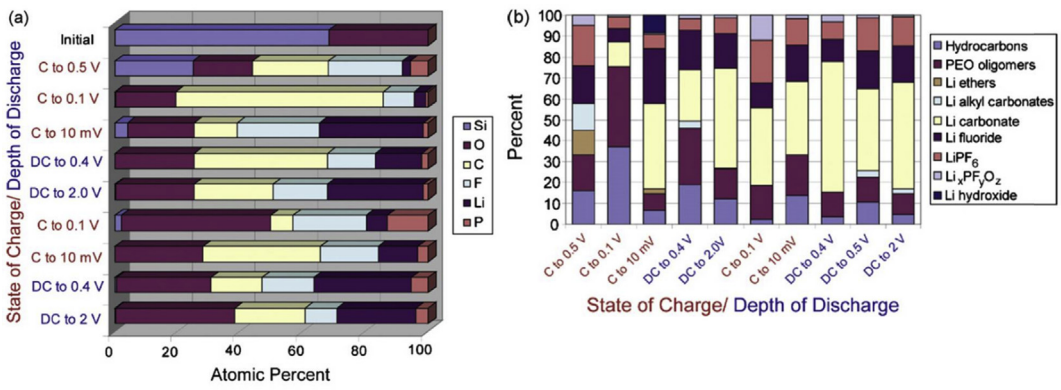


**Fig. 13.** Molecular species found on the surface of Si at different potentials as determined from high-resolution XPS scans [116]. Copyright (2009) Elsevier.

reactions. Some investigations have been done so far on the analysis of a gas type depending on the carbonate additives used. It was found that decomposition of FEC, VC, Chloroethylene Carbonate, DEC and EMC produces $CO_2$ [13,124,125], EC is responsible for a release of $C_2H_4$ and CO [124,126], PC decomposes with releasing a small amount of $C_2H_4$ [127]. During the online mass spectrometry measurement of a Li–Si thin film half-cell (in $LiNO_3$ electrolyte), a short release of $H_2$ and $N_2$ was observed, which lasted for a few initial lithiation cycles [128]. More likely that $H_2$ release is arising from the reduction of trace water in Si material or battery cell parts while $N_2$ is a result of $LiNO_3$ decomposition.

### 4.2. Solid state electrolytes

Solid state electrolytes (SSE) provide advantages in terms of simplicity of design and operational safety [129–131]. Solid electrolytes were proposed as a route to avoid dendrites formation in lithium batteries and for applications where elevated temperatures [132], as well as low temperatures, persist [129]. It is obvious that SSE can push towards designing safe nontoxic lithium-ion batteries with improved cycling performance and operation within a wide range of temperatures [133,134].

In case of Si, as shown above, it is essential to avoid the formation of nonuniform SEI layer and related capacity loss in the first cycle. Therefore, the capacity and cycling stability are expected to be improved. A 3D SS LIB with 1 μm lithium phosphorous oxynitride (LiPON) as a solid electrolyte (Fig. 14a) and 50 nm Si thin film anode exhibited a capacity of ~3500 mAh $g^{-1}$ with no decrease upon cycling for 60 cycles unlike the cell with a liquid electrolyte ($LPF_6$ in EC: DEC, $LiClO_4$ in PC) that was investigated for comparison purposes. SEM investigations did not reveal the SEI layer formation in the Si/LiPON interfacial region after cycling (Fig. 14b) [135].

The SS battery cell containing a-Si thin film anode (50–200 nm) with the LiPON electrolyte and a lithiated titanium oxysulfide ($Li_{1.2}TiO_{0.5}S_{2.1}$) cathode is shown in Fig. 15. Initially, upon testing a-Si thin film anode in a half-cell with solid electrolyte, the authors observed that the formation of $Li_{14}Si_4$ phase differs from that in liquid electrolytes, and this final reduction step occurs below 0 V at the low constant current or initiates only after 2 h floating at 0 V. The test results of batteries assembled with industrial tools and embedded in microelectronic packages demonstrated a stable cycle life (a capacity loss of only 0.006% per cycle) and ultrafast charge allowing to charge a battery up to 80% capacity within 1 min [136]. The incorporation of boron (B) into LiPON electrolyte (LiPONB) has enhanced chemical and thermal stability of the system. The Si thin film electrode with the LiPONB electrolyte demonstrated an excellent cycle life and coulombic efficiency with almost no loss during 1500 cycles. Besides, no cracks were observed in the film or at the electrode/electrolyte interface by SEM [137]. Investigation of the electrode-electrolyte interfacial region of the microbattery consisting of 600 nm Cu – 50 nm Si – LiPON –$LiCoO_2$ did not reveal any accumulation of Li atoms at the interface between anode and electrolyte, and alteration of electrical properties of Si–Cu layer upon cycling [138].

The 3D all solid-state LIB with 500 nm thick LiPON electrolyte, shown in Fig. 16, was assembled by deposition of corresponding layers on a designed 3D template. The cell demonstrated a poor power performance that was explained by the structural inhomogeneity of the layers, coupled with the low ionic conductivity of SSE and diffusion rate in the cathode, led to highly non-uniform internal current density distribution and poor cathode utilization [139].

In fact, there is a challenge with the deposition of SSE on an electrode and assembling a cell, especially if it is a 3D structure. In spite that some SSEs, in particular, thiophosphate-based, can reach the ionic conductivity comparable with that of liquid organic systems [140], the most of existing SSEs films derived by deposition demonstrated the ionic conductivity within $10^{-4} – 10^{-8}$ S $cm^{-2}$ which is not enough to surpass the batteries based on liquid electrolytes [130,131,141–148]. Another question is related to the mechanical stress that emerges inevitably in the SSE when Si volumetric changes occur during the processes of lithiation/delithiation. Currently, the further studies are required to investigate the stress in the fragile ceramic electrolytes as well as in the electrolyte-electrode interface.

## 5. Preparation techniques

There are various techniques available for thin film deposition. The preparation method and its conditions have a significant influence on the thin film microstructure, morphology, crystallinity, thin film-substrate interface/interphase purity, density and other physicochemical properties.

### 5.1. Physical methods

***Magnetron sputtering*** (MS) is based on physical vapor deposition and one of the most widespread processes employed for thin film manufacturing. In the working chamber of MS, the plasma-derived gas ions are accelerated between two electrodes in a low-pressure gas. The ions are directed towards the target surface where atoms of the latter are ejected from the material and flying on a substrate surface [149]. The benefits of MS are the easy control of film density, purity and thickness by varying power type (alternating current (radio frequency) – *rf*, direct current – *dc*), gas pressure, target material, rotation speed and deposition time, as well as an opportunity for the pre-sputtering cleaning of target and the further scale-up of the process. As a result, MS was quickly adapted for Si thin film preparation. A high purity disk-shaped Si is used as a target, and argon gas as a working gas. The sputtering power showed a significant effect on the value of the initial cycle

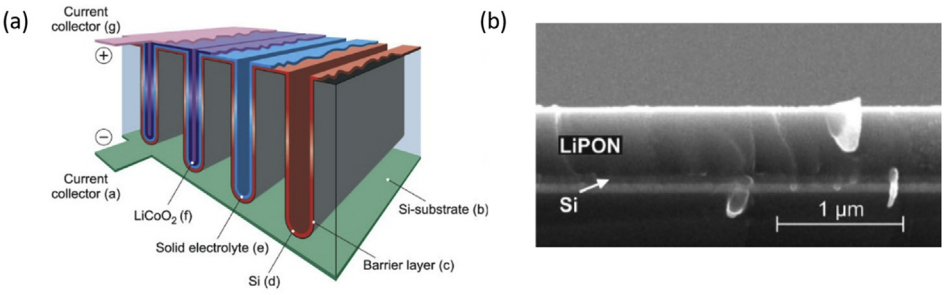


**Fig. 14.** (a) 3D integrated all-solid-state battery. (b) SEM image of Si/LIPON interface after cycling [135]. Copyright (2008) Willey.

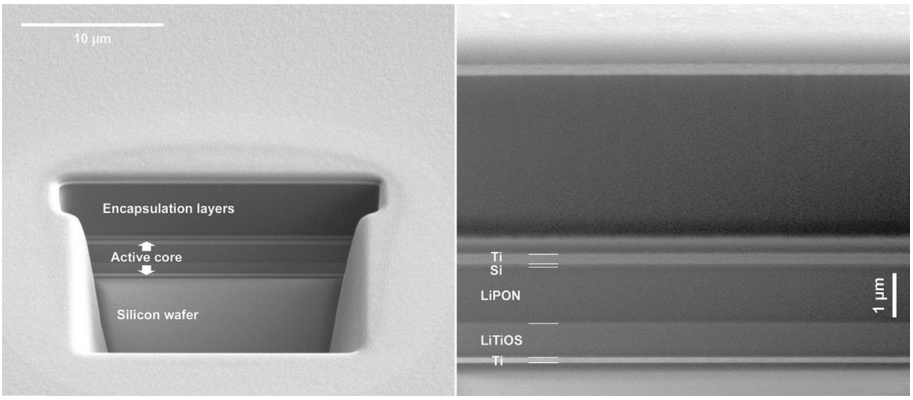


**Fig. 15.** FIB/SEM cross-section of a thin film encapsulated LIB comprising the $Li_{1.2}TiO_{0.5}S_{2.1}$/LiPON/Si active layers and titanium current collectors [136]. Copyright (2015) Willey.

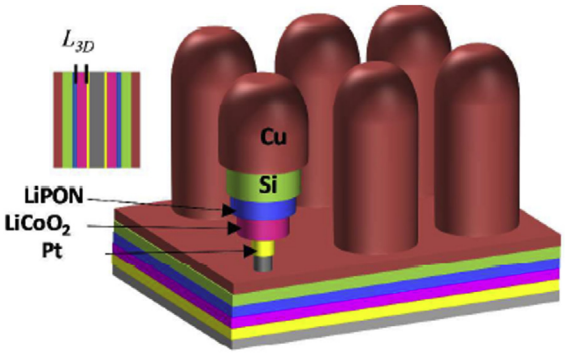


**Fig. 16.** Schematic of a 3D SSLIB [139]. Copyright (2016) American Chemical Society.

irreversible capacity of a prepared electrode. The comparison of samples prepared at three power values - 30, 60, 85 W, performed the initial specific capacity of 4200, 3800, 3060 mAh $g^{-1}$, respectively, i.e. the initial irreversible capacity of the anode increases as the power decreases. The reason was found to be a different Si oxide content, where a larger amount of oxygen incorporated in the film at lower power, and then led to the initial capacity drop due to the elevated amount of $Li_2O$ during SEI formation [49]. Heating the substrate up to 200 °C is found to strengthen the adhesion at the interface due to the interdiffusion of Si and Cu layers that finally resulted in the improved cyclability of the Si anode [47]. Among other approaches, substrate rotation option was added for better thickness uniformity, and deposition of Cr or Cu layer to improve attaching Si film to the substrate [61]. However, there are some drawbacks of MS. Firstly, the nonuniformity of film thickness, which is usually a bit thicker in the center of a substrate and thinner in the edges. Secondly, MS is not effective to prepare complicated 3D structures such as foams or wires because it sputters the faced surface only.

***Ion-beam deposition*** (IBD) is quite similar to MS apart from some differences. Unlike MS there is no bias applied and no plasma occurs between the target and the substrate in IBD. So due to that, conducting and non-conducting targets and substrates and even sensitive substrates can be applied. Finally, IBD operates at a much lower pressure (<0,013 Pa) than a standard MS, so the inclusion of sputter gas atoms in the film is a lesser problem [30,88,116,120,150].

Unlike MS, in ***pulsed laser deposition*** (PLD) technique the laser with high power pulses up to $10^8$ W $cm^{-2}$ is used in order to melt, evaporate and ionize material from the target surface. A highly luminous plasma plume is produced and expanded away towards to the substrate, on the surface of which the volatilized material deposits as a thin film [151]. The preparation of amorphous Si thin film by PLD was reported in several works [31,48,93,122]. Different deposition pressures were exploited in order to evaluate the influence of this process parameter on the morphological/electrochemical characteristics of the resulting nanostructures. The sample prepared at lower deposition pressure, having a higher porosity, featured by larger average pore size and lower surface area, showed better cycling performance.

***Vacuum evaporation*** (VE) is another effective method to prepare a-Si thin films [51–53,59]. Si powder or crushed pieces put in a tungsten heating boat usually serves as a Si source. Inside a work chamber with a low pressure of $10^{-4} - 10^{-5}$ Pa, electric current is passed through the tungsten boat to heat the Si source up to the melting point, and Si evaporates and deposits on a metallic substrate.

***Electron beam evaporation*** (EBE) differs from the previous method only in the way the source is heated – the electron beam gun is applied for this purpose. This method was successfully employed to prepare monolithic Si films and Si/Fe multilayer thin films [82,83,117,118].

***Ballistic consolidation*** (BC) and ***gas-phase condensation*** (GC) techniques were reported as well for Si films preparation. In the first process, the Si source was heated in a tungsten basket and evaporated into the gaseous media ($N_2 + H_2$) at the pressure of $2.6 \times 10^{-2}$ Pa. Further, the Si vapor was rapidly cooled to nucleate of nanocrystals due to a collision of the atoms that after formed the agglomerates due to the Brownian motion of nanocrystals in the gas. The gas was supplied through a nozzle, approaching the sound velocity, and the Si thin film grew from the ballistically consolidated nanoparticles when they hit the substrate at high speed. Thus, BC provides na opportunity to grow the thin film composed of nanocrystallites (5–20 nm). GC technique is quite similar to VE described above and provides an opportunity to obtain the entirely amorphous phase of Si. When comparing the cycling performance of two prepared films, a-Si anode confirmed its superiority.

### 5.2. Chemical methods

***Electrodeposition*** (ED) is a convenient and economically viable method for Si films preparation [75,152–155]. ED of Si films is carried out via a conventional ED procedure. The electrolyte usually contains a high purity silicon tetrachloride ($SiCl_4$) in propylene carbonate (PC) solvent. PC has a high dielectric constant and enhances dissolving the halide salts of silicon. The structure of electrodeposited Si film may vary from amorphous to a nanocrystalline structure. The different frequencies (0, 500, 1000, 5000 Hz) applied during ED were found to have an effect on the final performance of

**Table 2**
Electrochemical properties of a-Si thin film anode materials.

| N | Thin film structure | Preparation method (conditions) | Underlayer (nm)/ Substrate | Thickness (nm) | Cell (Electrolyte \|\| Counter electrode) | Voltage range, Current/C-rate | Reversible discharge specific capacity (mAh $g^{-1}$) | Number of cycles | Last discharge capacity (mAh $g^{-1}$) | Ref. |
|---|---|---|---|---|---|---|---|---|---|---|
| 1 | monolithic Si | MS (rf, 150 W, 0.67 Pa) | Ti(NA)/Cu | 35 | 1 M $LiPF_6$/EC:DEC (1:1) \|\| Li | 0.1–5 V, 125 <SUP>μ</SUP>A $cm^{-2}$ | 30 μAh | 50 | 18 μAh | [33] |
| 2 | monolithic a-Si | MS (rf, 200 W, 0.67 Pa) | Cu | 250<br>1000 | 1 M $LiPF_6$/EC:DMC (2:1) \|\| Li | 0.02–1.2 V, C/2.5 | 3800<br>3000 | 45<br>30 | 1800<br>1250 | [9,45] |
| 3 | monolithic a-Si | MS (dc, 150 W, 0.5 Pa) | St. steel | 400 | 1 M $LiPF_6$/EC:DMC (NA) \|\| Li | 0.2–2 V, 800 mA $g^{-1}$ | 900 | 60 | 785 | [46] |
| 4 | monolithic a-Si | MS (rf, 1.5 W/$cm^2$) | Cu | 1000–2000 | 1 M $LiPF_6$/EC:DMC (1:1) \|\| Li | 0.01–1 V, 100 <SUP>μ</SUP>A $cm^{-2}$ | 1750 | 30 | 1500 | [57] |
| 5 | monolithic a-Si | MS (rf, NA) | Cu | 200 | 1 M $LiPF_6$/EC:DEC (1:1) \|\| Li | 0.02–1.2 V, 0.5C | 3200 | 70–200 | 3000–1300 | [47] |
| 6 | monolithic a-Si | MS (rf, NA) | Cu | 800 | | | 1300 | 10 | 1400 | |
| 7 | monolithic a-Si | MS (rf, 60 W, 0.32 Pa) | Cu rough | 275 | 1 M $LiPF_6$/EC:DMC (1:1) +1% VC \|\| Li | 0–1.5 V, 0.5C | 2300 | 500 | 1700 | [25] |
| 8 | monolithic a-Si | MS (dc, 0.67 Pa) | St. steel | 100 | 1 M LiTFSI/MPPpTFSI \|\| Li | 3–4.3 V, C/16, C/10 | 3000 | 38 | 2750 | [55] |
| 9 | monolithic a-Si | MS (rf, 0.4 Pa, 200 °C) | Cu rough | 80 | 1 M $LiClO_4$/EC:DEC (1:1) \|\| Li | 5 mV - 1 V, 0.5C | 3000 | 80 | 2800 | [58] |
| 10 | monolithic a-Si | MS (rf, 50–100 W) | Cu nanowires | NA | 1 M $LiPF_6$/EC:DEC (1:1) \|\| Li | 0.01–1.5 V, 0.2C | 2303 | 60 | 2060 | [73] |
| 11 | monolithic a-Si | MS (rf, 100 W, 1 Pa) | St. steel | 100<br>200<br>500 | 1 M $LiPF_6$/EC:DMC (1:1) \|\| Li | 0.002–2 V, C/10 | 3800<br>3300<br>2000 | 30 | 3400<br>2850<br>1300 | [50] |
| 12 | monolithic a-Si | ED ($SiCl_4$/TBACl/PC, - 3.4 V vs. Pt, Ar, 20 °C) | Cu foam | 1500–4000 | 1.3 M $LPF_6$/EC:EMC (3:7) \|\| Li | 0.01–1.5 V, 50 <SUP>μ</SUP>A $cm^{-2}$ | ~950 | 60 | 920 | [75] |
| 13 | monolithic a-Si | LP-CVD ($SiH_4$/Ar/$H_2$, 200 sccm, 650 °C, 1333 Pa) | Ni porous (10 –50 μm) | 1200 | 1 M $LiPF_6$/EC:DMC (1:1) \|\| Li | 0.05–1.1 V, NA | 1000 | 20 | 200 | [8] |
| 14 | monolithic a-Si | CVD ($Si_2H_6$, 0.4 Pa, 450 °C) | Mo | ~50 | 1 M $LiClO_4$/PC \|\| Li | 0.1–3 V, 100 <SUP>μ</SUP>A $cm^{-2}$<br>0.2–3 V, 250 <SUP>μ</SUP>A $cm^{-2}$ | 3000<br>~3200 | 75<br>90 | ~0<br>3000 | [44] |
| 15 | monolithic a-Si | GC ($8 \cdot 10^{-4}$ Pa) | Ni | 100 | 1 M $LiPF_6$/EC:DMC (1:1) \|\| Li | 0–1.5 V, NA | 2500 | 50 | 1800 | [7] |
| 16 | monolithic a-Si | ED ($SiCl_4$/TBACl/PC, - 1.6 V vs. Pt, Ar, 20 °C) | Cu | 300–1000 | 1 M $LPF_6$/EC:DEC (1:2) \|\| Li | 0.02–1.2 V, 400 mA $g^{-1}$ | 1300 | 100 | 1260 | [153] |
| 17 | monolithic a-Si | EBE ($10^{-4}$ Pa) | Cu rough | 200 | 1.3 M $LiPF_6$/EC:DEC (3:7) +3% FEC \|\| Li | 0.05–2 V, 63.2 μAh $cm^{-2}$ | 3800 | 80 | 3450 | [118] |
| 18 | monolithic c-Si | MS (rf, 200 W, $3.4 \cdot 10^{-4}$ Pa) | Cu | 112<br>312 | 1 M $LiPF_6$/EC:DMC (1:1) \|\| Li | 0.01–1.5 V, 0.5C | 4200<br>4000 | 25 | 3150 | [24] |
| 19 | monolithic a-Si | EBE ($10^{-4}$ Pa) | Cu | 200 | 1.3 M $LiPF_6$/EC/DEC (3:7) \|\| Li<br>0.7 M LiBOB/EC/DEC (3:7) \|\| Li | 0.05–2 V, 0.2C | 3600<br>3600 | 100 | 1800<br>3000 | [117] |
| 20 | monolithic a-Si | PLD (500 °C, 5 Hz, 25 ns, 67 Pa, 3 J $cm^{-2}$) | St. steel | 1500 | 1 M $LPF_6$/EC:DMC (1:1) \|\| Li | 0.005–1.5 V(NA) | 19 μAh $cm^{-2}$ | 70 | 15 μAh $cm^{-2}$ | [48] |
| 21 | monolithic a-Si | PLD (20 °C, 10 Hz, $10^{-2}$ Pa, 150–160 J $cm^{-2}$) | St. steel | 120 | 1 M $LPF_6$/EC:DEC (1:1) \|\| Li | 0–1.5 V, 100 μA $cm^{-2}$ | 58 μAh $cm^{-2}$ | 50 | 55 μAh $cm^{-2}$ | [31] |
| 22 | monolithic a-Si | MS (dc) | NA | 6000 | 1 M $LiPF_6$/FEC:DMC (1:4) \|\| $LiNi_{0.5}Mn_{1.5}O_4$ | 0.01–1.2 V, C/8 | 140 | 150 | 125 | [119] |
| 23 | monolithic a-Si | PED ($SiCl_4$/TBACL/PC, 5000 Hz) | Cu | NA | 1 M $LiPF_6$/EC:DEC:FEC (45:45:10) \|\| Li | 0.01–1.2 V, 0.3 A $g^{-1}$ | 1200 | 500 | 805 | [154] |
| 24 | monolithic a-Si | LPCVD ($Si_2H_6$, 40 Pa and 450 °C) | Mo(300)/quartz | 50 | 1 M LiClO4/PC \| Li<br>1 M LiClO4/PC \|\| $LiMn_2O_4$ | 0-1 V, 100 μA $cm^{-2}$<br>3–4.4 V, 100 μA $cm^{-2}$ | 1300<br>330 | 300<br>400 | ~400<br>330 | [43] |
| 25 | monolithic a-Si | MS (dc, 0.34 W $cm^{-2}$, 0.5 Pa, Ar) | W(250)/Si wafer | 120 | Si \| LIPON \|\| LiTiOS | 0.05–1 V, 2C | 130 μAh $cm^{-2}$ | 1200 | 112 μAh $cm^{-2}$ | [136] |
| 26 | monolithic a-Si | MS (0.67 Pa, Ar) | Cu annealed | 330 | 1M$LPF_6$/EC:DEC (1:1) \|\| $LiFePO_4$/C | 2.5–4.4 V, 1C | 124 | 100 | 100 | [56] |
| 27 | monolithic c-Si | BC ($2.6 \cdot 10^{-2}$ Pa, 10% $H_2$+ 90% $N_2$) | Ni | 100 | 1 M $LiPF_6$/EC:DMC (1:1) \|\| Li | 0–1.5 V, NA | 1000 | 50 | 525 | [7] |
| 28 | monolithic c-Si | PLD (0.67 Pa, 200 °C, 3–4 mJ/$cm^2$, 10 Hz) | St. steel | 42 | 1 M $LPF_6$/EC:DEC (1:1) +5% $CH_3Si[OCH_3]_3$ \|\| Li | 0.1–1.5 V, 35 μA $cm^{-2}$, 1C | 2900 | 200 | 2400 | [122] |
| 29 | monolithic Si, n-type | IBS (rf, $4.5 \cdot 10^{-3}$ Pa) | Cu | 150 | 1 M $LiPF_6$/EC:DMC (1:1) +1% VC \|\| Li | 0–1.5 V, 0.05 mA $cm^{-2}$ | 2000 | 200 | 1900 | [120] |

(*continued on next page*)

**Table 2** (*continued*)

| N | Thin film structure | Preparation method (conditions) | Underlayer (nm)/ Substrate | Thickness (nm) | Cell (Electrolyte \|\| Counter electrode) | Voltage range, Current/C-rate | Reversible discharge specific capacity (mAh $g^{-1}$) | Number of cycles | Last discharge capacity (mAh $g^{-1}$) | Ref. |
|---|---|---|---|---|---|---|---|---|---|---|
| 30 | monolithic a-Si, n-type | PE-CVD (rf, 120 W/200 W, 4 Pa/10.7 Pa, $PH_3/SiH_4$/Ar, 200–400 °C) | Cu | 425–540 | 1 M $LiPF_6$/EC:DMC:DEC (1:1:1) \|\| Li | 0–1.5 V, 100 μA $cm^{-2}$ | 3800 | 50 | 2250 | [78] |
| 31 | monolithic a-Si, n-type | MS DC (0.34 W $cm^{-2}$, 0.5 Pa, Ar 100%, 13 nm $min^{-1}$) | Cu | 100–400 | 1 M $LiPF_6$/EC:PC:DMC (1:1:3) 2% of VC \|\| Li | 0.05–1 V, 100 μAh $cm^{-2}$, 2C | 39 μAh cm-2 | 1500 | 38 μAh $cm^{-2}$ | [137] |
| 32 | monolithic a-Si, n-type | VE (NA) | Ni | 50<br>150 | 1 M $LiClO_4$/PC \|\| Li | 0–2.5 V, 1C | 3750<br>2500 | 200 | 3850<br>2200 | [52] |
| 33 | monolithic Si, P-doped | VE (NA) | Ni rough | 1000 | 1 M $LiClO_4$/PC \|\| Li | NA | 2700 | 200 | 1750 | [59] |
| 34 | monolithic Si, P-doped | VE (NA) | Cu rough | 3600 | | NA | 2350 | 50 | 2100 | |
| 35 | monolithic a-Si, P-doped | VE($1.3 \cdot 10^{-5}$ Pa) | Ni rough | 50 | 1 M $LiClO_4$/PC \|\| Li | 0-2 V,<br>2C<br>12C<br>30C | 3600<br>3400<br>2300 | 200<br>900<br>2500 | 3600<br>3200<br>2200 | [53] |
| 36 | monolithic a-Si, P-doped | | Ni rough | 300<br>440 | 1 M $LiClO_4$/PC \|\| Li | 0-2 V,1C | 2300<br>2200 | 180<br>200 | 1900<br>2000 | |
| 37 | monolithic Si, P-doped | RF-PECVD (200 W, 10.6 Pa, $SiH_4$+$PH_3$, 150 °C) | Cu | 500–600 | $LiCF_3SO_3$/EC:PC/PAN:PVDF (gel-polymer) \|\| Li | 0.001–1.5 V, 0.3 C | 3150 | 50 | 2585 | [54] |
| 38 | monolithic a-Si, n-type | MS (rf, 85 W, 0.03 Pa) | St. steel | 200<br>550<br>1.1 | 1 M $LiPF_6$/EC:DEC (1:1) \|\| Li | 0.01–3 V, 500 mA $g^{-1}$ | 4400<br>3100<br>3000 | 50 | 4200<br>1000<br>700 | [49] |
| 39 | monolithic a-Si, n-type | MS (rf, 85 W, 0.03 Pa) | St. steel | 140 | | | 4200 | 20 | 4200 | |
| 40 | nanoporous a-Si, n-type | MS (rf, 85 W, 0.03 Pa) | St. steel | 450<br>750 | | | 3200<br>3100 | 20 | 2800<br>2400 | |
| 41 | nanopillars a-Si, n-type | MS (rf, 85 W, 0.03 Pa) | St. steel | 450<br>750 | | | 4000<br>3500 | 50 | 3900<br>4000 | |
| 42 | monolithic a-Si, B-doped | VE ($1 \cdot 10^{-5}$ Pa, deposition rate of 0.1 nm/min) | Ni | 77 | 1 M $LiClO_4$/PC \|\| Li | 0-2 V, 1 mV $s^{-1}$ | 1500 | 1250 | 1000 | [51] |
| 43 | a-Si, Cu-doped | MS(rf, 60 W, 0.67 Pa, | Cu | 220 | 1 M $LiPF_6$/EC:DEC (1:1) \|\| Li | 0-2 V, 20 μA $cm^{-2}$ | ~410 μAh $cm^{-2}$ $\mu m^{-1}$ | 40 | ~360 μAh $cm^{-2}\mu m^{-1}$ | [79] |
| 44 | monolithic a-Si/Cu (non-graded) | MS (NA, Si/Cu - 2200 W/ 350 W) | St. steel | ~3000 | 1 M $LiPF_6$/EC:DMC (1:1) \|\| Li | 0.2–1.2 V, C/12 | 1100 | 100 | 250 | [80] |
| 45 | monolithic a-Si/Cu (graded) | MS (NA, Si/Cu −50 W/350 W) | | | | | 1400 | 100 | 600 | |
| 46 | a-Si film, Cu-doped | IBS (2.5 kV, 40 mA) | Cu | 10000 | 1 M $LiPF_6$/EC:DMC (1:1) \|\| Li | 0.02–1.5 V, NA | 590 | 100 | 550 | [88] |
| 47 | monolithic a-Si + $O_2$ | MS (rf, 200 W, 0.45 Pa) | St. steel | 50<br>300 | $70Li_2S \cdot 30P_2S_5$ \|\| Li | 0.01–1.2 V, 0.1 mA $cm^{-2}$ | 2800<br>2800 | 100 | 2500<br>2000 | [133] |
| 48 | a-Si + 20% C and 20% $O_2$ | ED (SiCl4 in [BMP][TFSI], −2 V vs. Pt, Ar, 20 °C) | Cu | 1000–1200 | 1 M $LiPF_6$/EC:DMC (1:1) \|\| Li<br>1 M LiTFSI [BMP][TFSI] \|\| Li | 0.02–1.5 V, 0.1C | 1200<br>600 | 120<br>90 | 1080<br>500 | [155] |
| 49 | a-$SiMo_x$ alloy | MS (0.67 Pa, Ar) | Cu rough | 4000 | 1 M $LPF_6$/EC:DMC (1:1) \|\| Li | 0.01–1 V, 714 μA $cm^{-2}$ (0.2C) | 1319 | 100 | 1180 | [81] |
| 50 | monolithic a-Si:H | PECVD (rf, 250 °C, $SiH_4$, 13.56 MHz, 0.10 W $cm^{-2}$, 50 Pa and 33 sccm) | St. steel | 30 | 1 M LiClO4/PC \|\| Li | 0.125–2 V, 1C | 3500 | 100 | 2250 | [40]<br>[159] |
| 51 | monolithic c-Si:H | GD (hf, $SiH_4$, 100 °C)<br>GD (hf, $SiH_4$, 250 °C) | St. steel | 800<br>600 | NA | NA | 1000<br>1400 | 100 | 250<br>500 | [27] |
| 52 | monolithic c-Si:H | GD (hf, $SiH_4$, 250 °C) | St. steel | 250 | 1 M $LiClO_4$/PC:DMC (7:3) \|\| Li | 0–1.2 V, 0.07 mA | 2900 | NA | NA | [121] |
| 53 | monolithic Si, 2-layer monolithic Si, 4-layer | MS (dc, 200 W, $1.5 \cdot 10^{-3}$Pa/ $1.5 \cdot 10^{-4}$Pa) | Cr(20)/Cu | 190<br>380 | 1.2 M $LiPF_6$/EC:EMC (3:7) \|\| Li | 10 mV-1.5 V, 40 μA/$cm^2$ | ~1800<br>~2000 | 50 | 1392<br>1704 | [61] |
| 54 | monolithic Si multilayer | MS (rf, 100 W, 1 Pa, periodic/constant bias) | Cr(10)/Cu | 696<br>618 | 1 M $LiPF_6$/EC:DEC (1:1) \|\| Li | 0.01–1 V, 0.2C | 2050<br>1500 | 100 | 1905<br>600 | [62] |
| 55 | lozenge-patterned Si | MS (dc, 0.67 Pa) | St. steel | 350 | 1 M $LiPF_6$/EC:DEC (1:1) \|\| Li | 0.01–1.2 V 0.5C | 2200 | 120 | 1650 | [63] |
| 56 | lozenge-patterned Si | MS (dc, 0.67 Pa) | St. steel rough | 350 | 1 M $LiPF_6$/EC:DMC (1:1) \|\| Li | 0.01–1.2 V, 0.2C | 2250 | 100 | 2050 | [64] |

| | | | | | | | | | | |
|---|---|---|---|---|---|---|---|---|---|---|
| 57 | honeycombs a-Si | PECVD (rf, 350 W, 300 °C, SiH 4 + PH 3 + H 2, 1.6 mbar) + Lithography | TiN | 1100 | 1 M $LiClO_4$/PC \|\| Li | 0.1–0.8 V, 75 μA $cm^{-2}$ | 52 μAh $cm^{-2}$ | 70 | 32 μAh $cm^{-2}$ | [69] |
| 58 | hills-like a-Si | VE ($7.5 \cdot 10^{-3}$ Pa) | Cu rough | 6000 | 1 M $LPF_6$/EC:DEC:DMC (1:1:1) \| Li | 0.01–2.0 V, μA $cm^{-2}$ | 1220 | 20 | 1050 | [60] |
| 59 | patterned a-Si | MS (NA) | Cu patterned | 560 | 1 M $LPF_6$/EC:DMC (1:1) \|\| Li | 0–1.5 V, 0.5 C | 2800 | 100 | 2100 | [66] |
| 60 | Si nanowires | ED ($SiCl_4$/TBACl/PC, −2.4 V vs. Pt) | 3D TMV/Ni on SS | 80 | NA | 0.01–1.5 V, 0.25C | 2300 | 173 | 1200 | [77] |
| 61 | 3D Si anode | LPCVD ($SiH_4$, 33.3 Pa, 610 °C) | TiN | 50 | 1 M $LiPF_6$ \| EC:DEC \|\| Li<br>1 M $LiClO_4$/PC \|\| Li<br>LIPON (1 μm) \|\| Li | 0-3 V, 1C | 3500<br>3600<br>3500 | 60 | 1200<br>~2350<br>3500 | [135] |
| 62 | a-Si-graphene/carbon nanotubes | MS (rf, 0.5 Pa, 150 W) | graphene & carbon nanotubes paper | 13000 | 1 M $LiPF_6$/EC:DEC (1:1) \|\| Li | 0.01–2.5 V, 100 mAh $g^{-1}$ | 1417 | 100 | 425 | [103] |
| 63 | porous c-Si nanowires, B-doped | Etching of Si wafers ($HF + AgNO_3$, 3 h) | Si wafer | Diameter and wall ~ 8 | NA | 0.01–2.0 V,<br>0,15C<br>0.3C<br>0.6C<br>0.9C<br>1.2C<br>2.4C | 3700<br>2600<br>2000<br>1900<br>1700<br>1300 | 20 | 3500<br>2500<br>2000<br>1900<br>1700<br>1300 | [72] |
| 64 | Si nanowires | Vapour–Liquid–Solid growth ($SiH_4$+Ar, $5.3 \cdot 10^3$ Pa, 485 °C, 20 min) | Au(seeds)/St. steel | 100 (diam.)<br>10000 (length) | 1 M LiPF6/EC:DEC (1:1) \|\| Li | 0.07–0.7 V, C/5<br>0.07–2 V, C/5 | 1700<br>2500 | 80 | 2000<br>1300 | [42] |
| 65 | Si porous, n-type | MS (rf, 80 W, 0.66 Pa) | porous Cu | 400 | 1 M $LiPF_6$/DEC:EC:EMC (1:1:1) \|\| Li | 0.1–1.5 V, 30 μA $cm^{-2}$ | 76 μA $cm^{-2}$ | 100 | 67 μA $cm^{-2}$ | [74] |
| 66 | c-Si ribbons | – | Cr(5)/Au(100)/ Cr(5)/PDMS | 400 | 1 M $LiPF_6$/EC:DEC (1:1) \|\| Li | 0.005–3 V, C/4 | 4137 | 500 | 3498 | [68] |
| 67 | Cu-coated a-Si | MS (rf, 200 W, 0.667 Pa) | Cu(300)/Cu | 500 | 1.2 M $LiPF_6$/EC:DEC (3:7) + 10% FEC \|\| Li | 0.01–1.2 V, 25 μA $cm^{-2}$ | 2100 | 60 | 1900 | [90] |
| 68 | Si/Cu multilayer | MS (NA) | Cu | Si/Cu:50/400 | LiPON \|\| $LiCoO_2$ | 30 nA | 16 μAh $cm^{-2}$ | 100 | 14 μAh $cm^{-2}$ | [138] |
| 69 | $Cu_2O$-coated Si | ECR-MOCVD (1.33 Pa, 200 °C) | Cu | $Cu_2O$/Si: 200/800 | 1 M $LiPF_6$ EC:EMC:DC (1:1:1) \|\| Li | 0-2 V, 1C | 1630 | 100 | 500 | [91] |
| 70 | C-coated a-Si:H | RF-PECVD (200 W, 1.3 Pa, $SiH_4$, 150 °C) + MS ($C_{60}$, 300 W) | Cu | NA | 1 M $LPF_6$ EC:DEC:DMC (1:1:1) \|\| Li | 0-2 V, 100 μA $cm^{-2}$ | 3500 | 100 | 1200 | [160] |
| 71 | composite a-Si/B | MS (rf/dc, 110 W/150 W, 0.13 Pa) | Cu | NA | 1 M $LiPF_6$/EC:DEC:FEC (3:6:1) \|\| Li | 0.005–0.9 V, C/5 | 3250 | 3 | 3250 | [85] |
| 72 | composite a-Si/Ti | MS (Si – rf, 20–40 W; Ti – dc, 150 W, 0.5 Pa) | Ti(320)/quartz | Ti:Si<br>60 (1:8.78)<br>30 (1:8.79)<br>30 (1:8.89) | 1 M $LiPF_6$/EC:DMC (1:1) \|\| Li | NA | 250 μAh<br>140 μAh<br>310 μAh | 20 | 200 μAh<br>140 μAh<br>290 μAh | [89] |
| 73 | monolithic Si | MS (rf, NA) | Cr(10)/Cu | 250 | 1 M $LiPF_6$/EC:DEC (1:2) \|\| Li | 0.02–1.2 V, 100–500 μA $cm^{-2}$ | 2822 | 75 | ~800 | [92] |
| 74 | composite Si/C bilayer | | | 50/250 | | | 2509 | | ~2450 | |
| 75 | composite C/Si/C tri-layer | | | 50/250/50 | | | 2025 | | ~1900 | |
| 76 | C-coated a-Si algae | PLD (20 Hz, 60–100 Pa, 5 J/$cm^2$) | Cu | 1000 | 1 M $LPF_6$/EC:DEC (1:1) \|\| Li | 0.005–1.5 V, 54 μA $cm^{-2}$ | 80 μAh $cm^{-2}$ | 1000 | 80 μAh $cm^{-2}$ | [95] |
| 77 | composite Si/C multilayered | PLD (Si – 40 Pa, C- 5 Pa), annealing (400 °C) | Cu | 1000 | 1 M $LiPF_6$/EC:DMC (1:1) \|\| Li | 0.02–1.5 V, 130 μA $cm^{-2}$ | 300 μAh $cm^{-2}$ | 100 | 85 μAh $cm^{-2}$ | [93] |
| 78 | composite C/Si | MS ($5 \cdot 10^{-3}$ mbar, 20 °C, Si –88 W, C – 40 W) | Cu | 5/140 10/140 50/140 | 1 M $LiPF_6$/EC:DEC (3:7) +2% VC \|\| Li | 0.04–1.5 V 1C | 2750<br>3000<br>3250 | 150 | 2400<br>2500<br>2750 | [29] |
| 79 | composite Si/C/Si | | | 70/5/70 70/10/ 70<br>70/50/70 | | | 2900<br>3000<br>3300 | | 2600<br>2600<br>2750 | |

(*continued on next page*)

**Table 2** (*continued*)

| N | Thin film structure | Preparation method (conditions) | Underlayer (nm)/ Substrate | Thickness (nm) | Cell (Electrolyte \|\| Counter electrode) | Voltage range, Current/C-rate | Reversible discharge specific capacity (mAh $g^{-1}$) | Number of cycles | Last discharge capacity (mAh $g^{-1}$) | Ref. |
|---|---|---|---|---|---|---|---|---|---|---|
| 80 | composite a-Si/C multilayers | MS (rf(Si), dc(C), 300 W, 1 Pa) | Cu | Si:C<br>500(5:1)<br>500 (6:1)<br>500(7:1)<br>1100(5:1)<br>1300(5:1) | 1 M $LiPF_6$/EC:DMC \|\| Li | 0.01–1.2 V, 1C | 2100<br>2050<br>1300<br>100<br>300 | 200 | 2500<br>2000<br>250<br>1900<br>1700 | [98] |
| 81 | composite Si/$C_{60}$ | RF-PECVD (200 W, 10.6 Pa, $SiH_4$, 150 °C) | Cu | 300 | 1 M $LPF_6$/EC:DEC:DMC (1:1:1) \|\| Li | 0–2 V, 1500 μA $cm^{-2}$ | 2000 | 30 | 2500 | [94] |
| 82 | composite Si/graphene | PLD for Si (<1.3 × $10^{-5}$ Pa) CVD for graphene ($CH_4$, 1050 °C), | Ni | graphene/Si<br>23/6.35 | 1 M $LiPF_6$/DC:DEC (1:1) \|\| Li | 0.01–3.0 V, C/10 to C/1.5 | 2400 | 100 | NA | [107] |
| 83 | Ti/Si/Ti multilayers | MS (0.5 Pa, 100 W) | Cu | Ti/Si/Ti<br>8/150/8<br>16/150/16<br>24/150/24<br>32/150/32<br>40/150/40 | 1 M $LiPF_6$/EC:DEC (1:1) \|\| Li | 0.01–2.0 V, 30 μA $cm^{-2}$ | 2250<br>2060<br>1875<br>1750<br>1625 | 30 | 1875<br>1690<br>1500<br>1375<br>1250 | [87] |
| 84 | Al-coated Si/Cu/Ti multilayers (with $Cu_3Si$ nanowires) | MS (rf, 0.5 Pa, 60 W) | Cu(300)-Ti(400)/ quartz | Al/Si<br>0/400<br>2/400<br>4/400<br>8/400 | 1 M $LiPF_6$/EC:DMC (1:1) \|\| Li | 0.005–2 V, 20 μA $cm^{-2}$ | 1500<br>1000<br>1000<br>1000 | 100 | 1375<br>875<br>750<br>125 | [99] |
| 85 | composite Si–Y multilayer | MS (rf, 0.5 Pa, 300 °C) | Cu | Y/Si/Y/Si:<br>Si – 225; Y:<br>15<br>22.5<br>30<br>37.5 | 1 M $LiPF_6$/EC:DEC(1:1) \|\| Li | NA | 2800<br>2850<br>2500<br>2300 | 50 | 2250<br>2500<br>2050<br>1800 | [86] |
| 86 | SiN-coated Si | Sputtering (dc, 80 W, Ar) | Cu micro-cone arrays | 7.7<br>15.4<br>23.1 | 1 M $LiPF_6$/EC:EMC (1:1) \|\| Li | 0.05–1.2 V, 0.2C | 2750<br>1800<br>1600 | 200 | 1250<br>750<br>800 | [96] |
| 87 | composite a-Si-Fe multilayers | EBE (NA) | Cu | 245.5 | 1 M $LPF_6$/EC:DEC (1:1) \|\| Li | 0–1.2 V, 30 μA $cm^{-2}$ | 140 μAh $cm^{-2}$ | 50 | 125 μAh $cm^{-2}$ | [82] |
| 88 | Ti/Si/Fe multilayers | EBE (NA) | Ni etched carbon-fiber on St. steel | 150/2000/400 | 1 M $LiPF_6$/EC:DEC (1:1) \|\| Li | 0–1.2 V, 200 μA $cm^{-2}$ | 450 μAh $cm^{-2}$ | 50 | 450 μAh $cm^{-2}$ | [83] |
| 89 | 3D a-Si, n-type/carbon fiber | MS (rf, 1.33 Pa, Ar) | | Diameter 3000 – 5000 | 1 M $LiPF_6$/EC:EMC (1:2) \|\| Li | 0.01–1.5 V, 3750 μA$cm^{-2}$ | ~1750 | 200 | 1000 | [105] |
| 90 | a-Si,n-type/graphene/ Ni foam | MS for Si (rf, 80 W, 0.66 Pa) CVD for graphene ($CH_4$, 1050 °C) | Ni foam | 50–400 | 1 M $LPF_6$/EC:DEC:EMC (1:1:1) \|\| Li | 0.1–1.5 V, 30 μA $cm^{-2}$ | 141 | 500 | 75 | [104] |
| 91 | 3D a-Si, n-type/Co nanosheets | MS (rf, 60 W, 1.07 Pa) | Co/Ni | NA | 1 M $LiPF_6$/EC:DEC (1:1) \|\| Li | 0–1.5 V,<br>0.1, 0.5, 1.2, 5C | 2340 | 100 | 1910 | [76] |
| 92 | 3D Si/Al multilayers | MS (rf, 300 W, 0.75 Pa, Ar) | Cu nanoribbons | 1000 | 1 M $LPF_6$/EC:DMC:DEC (1:1:1) +2% VC \|\| Li<br>1 M $LiPF_6$/EC:DMC:DEC (1:1:1) +2% VC + 10% FEC \|\| Li | 0.1–1.2 V, 4.2 A $g^{-1}$ (1C)<br>0.1–1.2 V, 2.1 A $g^{-1}$ (C/2) | 1170<br>~1800 | 120<br>300 | 1015<br>1175 | [84] |

battery cell. It was shown that the higher frequencies result in a better stability and performance of the thin film. The Si thin film electrodeposited at 5000 Hz pulse current frequency demonstrated a stable capacity of 805 mAh $g^{-1}$ with a capacity loss of ~0.056% per cycle upon 500 cycles that was explained by the enhanced stability of the film. Besides, it was fixed that the crack size of the thin film during cycling is decreasing with increase in frequency. This difference is most likely due to a change in the mechanisms of nucleation and growth of thin films formed at different frequencies [154]. In contrast with other methods, ED allows the internal surfaces of complicated 3D structures to be easily coated with a relatively good uniformity [75,77]. However, a high irreversible loss at the first cycle as the result of the loss of $Li^+$ ions due to the presence of oxygen incorporated into the film remains the big problem of electrodeposited Si thin film.

***Chemical vapor deposition*** (CVD) is a deposition technique which allows obtaining the high quality and purity thin films [156]. There are various modifications like low pressure CVD (LPCVD) [43], reduced pressure CVD [157] and plasma enhanced CVD (PECVD) [69,78,100,158] etc. This method is based on a chemical decomposition of Si-containing gas like $SiH_4$ or disilane ($Si_2H_6$) at high temperatures following the adsorption of the released atoms or molecules on the substrate surface. Effect of substrate temperature on electrochemical characteristics of the Si film anode obtained by PECVD was studied by Song et al. [78]. It was found that during the deposition on Cu substrate under the elevated temperatures above 400 °C, the reaction between Si radicals and diffused Cu ions took place with the formation of the granular shaped Cu silicide particles. The thin film anode exhibited an improved cyclability thanks to the formed phase, which mitigated the volume change owing to the existence of additional chemical bonding and reduced electrical resistance.

***Glow discharge plasma deposition*** (GDPD) of Si thin films is a mixed physicochemical process. Plasma is generated when the voltage is applied between two oppositely charged metal electrodes and the electric current is passed through a low-pressure gas. The hydrogenated a-Si films (a-Si:H) were obtained via decomposition of silane ($SiH_4$) gas in a glow discharge plasma at high temperatures. An increase in the synthesis temperature has been found to decrease the residual hydrogen content in the films. The density of the material observed to be lower at the lower deposition temperature. The a-Si:H thin films obtained at the higher temperature (100 °C vs. 250 °C) showed an improved electrochemical performance [27,28,121].

## 6. Summary

For the last two decades, the number of studies on Si thin film anodes has significantly increased, leading to the better understanding of factors affecting the electrochemical performance these anodes. There were acquired the insights on the mechanism of $Li^+$ ions insertion into Si, their possible paths inside the Si thin film anode, the importance of an electrode-substrate interface and SEI layer formation.

The best results from Table 2 point on a group of the most prospective routes for further successful development and commercialization of the Si thin film anode. Thus, the choice of the appropriate electrolyte, enhancement of the adhesion between the film and the current collector, doping incorporation can stabilize the capacity retention and prolong cycle life of a battery.

The focus of the recently reported works was made mainly on the design of 3D structured Si anodes and modification of electrolytes, in particular, the design of SS cell. 3D structures in anode are capable to release stresses and accommodate volume expansion and achieve high current rates and power density. Meanwhile, SSEs with high ionic conductivity and stress resistivity are promising as the solution of problems with nonuniform SEI layer.

To sum up, we have provided an informative review on many aspects of Si thin film anodes such as the lithiation/delithiation mechanisms, fading behaviors, current research progress and the basics of the preparation methods. To apply Si thin film in LIMBs as soon as possible, facing the current situation and resolving the problems are necessary. Therefore, in order to develop a high-performance Si thin film anode, this review objectively summarizes the issues and challenges that will help scientist to understand the actual status of Si thin films and find new solutions to its further development.

## Acknowledgements

The authors acknowledge financial support from the Ministry of Education and Science of the Republic of Kazakhstan by the research grant AP05133519 “Development of 3-dimensional thin film silicon based anode materials for next-generation lithium-ion microbatteries” and the Targeted Program BR05236524 “Innovative materials and systems for energy conversion and storage”. A.M. thanks the PhD Program Grant from the Ministry of Education and Science of the Republic of Kazakhstan.

## References

[1] X. Zuo, J. Zhu, P. Müller-Buschbaum, Y.-J. Cheng, Silicon based lithium-ion battery anodes: a chronicle perspective review, Nanomater. Energy 31 (2017) 113–143.
[2] W.J. Zhang, A review of the electrochemical performance of alloy anodes for lithium-ion batteries, J. Power Sources 196 (2011) 13–24.
[3] P. Meister, H. Jia, J. Li, R. Kloepsch, M. Winter, T. Placke, Best practice: performance and cost evaluation of lithium ion battery active materials with special emphasis on energy efficiency, Chem. Mater. 28 (2016) 7203–7217.
[4] M.N. Obrovac, L.J. Krause, Reversible cycling of crystalline silicon powder, J. Electrochem. Soc. 154 (2007) A103–A108.
[5] M.N. Obrovac, L. Christensen, Structural changes in silicon anodes during lithium insertion/extraction, Electrochem. Solid State Lett. 7 (2004) A93–A96.
[6] J.Y. Kwon, J.H. Ryu, S.M. Oh, Performance of electrochemically generated $Li_{21}Si_5$ phase for lithium-ion batteries, Electrochim. Acta 55 (2010) 8051–8055.
[7] J. Graetz, C.C. Ahn, R. Yazami, B. Fultz, Highly reversible lithium storage in nanostructured silicon, Electrochem. Solid State Lett. 6 (2003) A194–A197.
[8] S. Bourderau, T. Brousse, D. Schleich, Amorphous silicon as a possible anode material for Li-ion batteries, J. Power Sources 81–82 (1999) 233–236.
[9] J.P. Maranchi, A.F. Hepp, P.N. Kumta, High capacity, reversible silicon thin-film anodes for lithium-ion batteries, Electrochem. Solid State Lett. 6 (2003) A198–A201.
[10] A. Casimir, H. Zhang, O. Ogoke, J.C. Amine, J. Lu, G. Wu, Silicon-based anodes for lithium-ion batteries: effectiveness of materials synthesis and electrode preparation, Nanomater. Energy 27 (2016) 359–376.
[11] H.-C. Shin, J. a. Corno, J.L. Gole, M. Liu, Porous silicon negative electrodes for rechargeable lithium batteries, J. Power Sources 139 (2005) 314–320.
[12] N.D. Lithiation, X.H. Liu, L. Zhong, S. Huang, S.X. Mao, T. Zhu, J.Y. Huang, Size-dependent fracture of silicon nanoparticles during lithiation, ACS Nano 6 (2012) 1522–1531.
[13] R. Jung, M. Metzger, D. Haering, S. Solchenbach, C. Marino, N. Tsiouvaras, C. Stinner, H.A. Gasteiger, Consumption of fluoroethylene carbonate (FEC) on Si-C composite electrodes for Li-Ion batteries, J. Electrochem. Soc. 163 (2016) A1705–A1716.
[14] J. Chen, Recent progress in advanced materials for lithium ion batteries, Materials (Basel) 6 (2013) 156–183.
[15] N.J. Dudney, Thin film micro-batteries, Electrochem. Soc. Interface 17 (2008) 44–48.
[16] S. Ferrari, M. Loveridge, S.D. Beattie, M. Jahn, R.J. Dashwood, R. Bhagat, Latest advances in the manufacturing of 3D rechargeable lithium microbatteries, J. Power Sources 286 (2015) 25–46.
[17] S.D. Jones, J.R. Akridge, F.K. Shokoohi, Thin film rechargeable Li batteries, Solid State Ionics 69 (1994) 357–368.
[18] U. Kasavajjula, C. Wang, A.J. Appleby, Nano- and bulk-silicon-based insertion anodes for lithium-ion secondary cells, J. Power Sources 163 (2007) 1003–1039.
[19] J.R. Szczech, S. Jin, Nanostructured silicon for high capacity lithium battery anodes, Energy Environ. Sci. 4 (2011) 56–72.

[20] T.D. Hatchard, J.R. Dahn, In Situ XRD and electrochemical study of the reaction of lithium with amorphous silicon, J. Electrochem. Soc. 151 (2004) A838.
[21] D. Ma, Z. Cao, A. Hu, Si-based anode materials for Li-ion batteries: a mini review, Nano-Micro Lett. 6 (2014) 347–358.
[22] P. Limthongkul, Y. Il Jang, N.J. Dudney, Y.M. Chiang, Electrochemically-driven solid-state amorphization in lithium-metal anodes, J. Power Sources 119–121 (2003) 604–609.
[23] A. Bordes, E. De Vito, C. Haon, C. Secouard, A. Montani, P. Marcus, Investigation of lithium insertion mechanisms of a thin-film Si electrode by coupling time-of-flight secondary-ion mass spectrometry, x-ray photoelectron spectroscopy, and focused-ion-beam/SEM, ACS Appl. Mater. Interfaces 7 (2015) 27853–27862.
[24] H. Guo, H. Zhao, C. Yin, W. Qiu, A nanosized silicon thin film as high capacity anode material for Li-ion rechargeable batteries, Mater. Sci. Eng. B 131 (2006) 173–176.
[25] L.B. Chen, J.Y. Xie, H.C. Yu, T.H. Wang, An amorphous Si thin film anode with high capacity and long cycling life for lithium ion batteries, J. Appl. Electrochem. 39 (2009) 1157–1162.
[26] K. Yoshimura, J. Suzuki, K. Sekine, T. Takamura, Evaluation of the Li insertion/extraction reaction rate at a vacuum-deposited silicon film anode, J. Power Sources 146 (2005) 445–447.
[27] T.L. Kulova, Y.V. Pleskov, A.M. Skundin, E.I. Terukov, O.I. Kon'kov, Lithium intercalation into amorphous-silicon thin films: an electrochemical-impedance study, Russ. J. Electrochem. 42 (2006) 708–714.
[28] T.L. Kulova, A.M. Skundin, Y.V. Pleskov, O.I. Kon, The Li insertion/extraction characteristics of amorphous silicon thin films, Chembiochem Q 21 (2007) 83–92.
[29] A. Reyes Jiménez, R. Klöpsch, R. Wagner, U.C. Rodehorst, M. Kolek, R. Nölle, M. Winter, T. Placke, A step toward high-energy silicon-based thin film lithium ion batteries, ACS Nano 11 (2017) 4731–4744.
[30] F. Strauß, E. Hüger, P. Heitjans, T. Geue, J. Stahn, H. Schmidt, Lithium permeation through thin lithium-silicon films for battery applications investigated by neutron reflectometry, Energy Technol. 4 (2016) 1582–1587.
[31] H. Xia, S. Tang, L. Lu, Properties of amorphous Si thin film anodes prepared by pulsed laser deposition, Mater. Res. Bull. 42 (2007) 1301–1309.
[32] A.A. Arie, J.K. Lee, Estimation of Li-Ion diffusion coefficients in C60 coated Si thin film anodes using electrochemical techniques, Defect Diffusion Forum 326–328 (2012) 87–92.
[33] S.J. Lee, J.K. Lee, S.H. Chung, H.Y. Lee, S.M. Lee, H.K. Baik, Stress effect on cycle properties of the silicon thin-film anode, J, Power Sources 97–98 (2001) 191–193.
[34] Y. Gwak, J. Moon, M. Cho, Multi-scale analysis of an electrochemical model including coupled diffusion, stress, and nonideal solution in a silicon thin film anode, J. Power Sources 307 (2016) 856–865.
[35] K. Zhao, ES240 Final Project: FEM Study on Intercalation-induced Stress Level in Amorphous Si Thin Film Anode of Lithium-ion Battery, Cambridge, 2008.
[36] S. Pal, S.S. Damle, P.N. Kumta, S. Maiti, Modeling of lithium segregation induced delamination of a-Si thin film anode in Li-ion batteries, Comput. Mater. Sci. 79 (2013) 877–887.
[37] S.H. Patel, Numerical Modeling of the Failure Mechanisms in Si Thin Film Anode for Li-ion Batteries, Michigan Technological University, 2011.
[38] J. Shaffer, P. Peralta, Finite Element Analysis of Silicon Thin Films on Soft Substrates as Anodes for Lithium Ion Batteries, Arizona State University, 2011.
[39] B. Jerliu, E. Hüger, L. Dörrer, B.K. Seidlhofer, R. Steitz, V. Oberst, U. Geckle, M. Bruns, H. Schmidt, Volume expansion during lithiation of amorphous silicon thin film electrodes studied by in-operando neutron reflectometry, J. Phys. Chem. C 118 (2014) 9395–9399.
[40] C. Pereira-Nabais, J. Światowska, M. Rosso, F. Ozanam, A. Seyeux, A. Gohier, P. Tran-Van, M. Cassir, P. Marcus, Effect of lithiation potential and cycling on chemical and morphological evolution of si thin film electrode studied by ToF-SIMS, ACS Appl. Mater. Interfaces 6 (2014) 13023–13033.
[41] B. Breitung, P. Baumann, H. Sommer, J. Janek, T. Brezesinski, In situ and operando atomic force microscopy of high-capacity nano-silicon based electrodes for lithium-ion batteries, Nanoscale 8 (2016) 14048–14056.
[42] R. Ruffo, S.S. Hong, C.K. Chan, R.A. Huggins, Y. Cui, Impedance analysis of silicon nanowire lithium ion battery anodes, J. Phys. Chem. C 113 (2009) 11390–11398.
[43] H. Jung, M. Park, S.H. Han, H. Lim, S.K. Joo, Amorphous silicon thin-film negative electrode prepared by low pressure chemical vapor deposition for lithium-ion batteries, Solid State Commun. 125 (2003) 387–390.
[44] H. Jung, M. Park, Y.G. Yoon, G.B. Kim, S.K. Joo, Amorphous silicon anode for lithium-ion rechargeable batteries, J. Power Sources 115 (2003) 346–351.
[45] J.P. Maranchi, A.F. Hepp, a. G. Evans, N.T. Nuhfer, P.N. Kumta, Interfacial properties of the a-Si/Cu:active–inactive thin-film anode system for lithium-ion batteries, J. Electrochem. Soc. 153 (2006) A1246–A1253.
[46] U. Tocoglu, T. Cetinkaya, O. Cevher, M.O. Guler, H. Akbulut, Nanostructured silicon thin film electrodes for li-ion batteries, Acta Phys. Pol. A 123 (2013) 380–382.
[47] T. Moon, C. Kim, B. Park, Electrochemical performance of amorphous-silicon thin films for lithium rechargeable batteries, J. Power Sources 155 (2006) 391–394.
[48] M.S. Park, G.X. Wang, H.K. Liu, S.X. Dou, Electrochemical properties of Si thin film prepared by pulsed laser deposition for lithium ion micro-batteries, Electrochim. Acta 51 (2006) 5246–5249.
[49] R.S. Omampuliyur, M. Bhuiyan, Z. Han, Z. Jing, L. Li, E.A. Fitzgerald, C. V Thompson, W.K. Choi, Nanostructured thin film silicon anodes for Li-Ion microbatteries, J. Nanosci. Nanotechnol. 15 (2015) 4926–4933.
[50] J. Li, A.K. Dozier, Y. Li, F. Yang, Y.-T. Cheng, Crack pattern formation in thin film lithium-ion battery electrodes, J. Electrochem. Soc. 158 (2011) A689–A694.
[51] S. Ohara, J. Suzuki, K. Sekine, T. Takamura, Li insertion/extraction reaction at a Si film evaporated on a Ni foil, J. Power Sources 119–121 (2003) 591–596.
[52] S. Ohara, J. Suzuki, K. Sekine, T. Takamura, A thin film silicon anode for Li-ion batteries having a very large specific capacity and long cycle life, J. Power Sources 136 (2004) 303–306.
[53] T. Takamura, S. Ohara, M. Uehara, J. Suzuki, K. Sekine, A vacuum deposited Si film having a Li extraction capacity over 2000 mAh/g with a long cycle life, J. Power Sources 129 (2004) 96–100.
[54] A.A. Arie, J.K. Lee, Electrochemical properties of P-Doped silicon thin film anodes of lithium ion batteries, Mater. Sci. Forum 737 (2013) 80–84.
[55] V. Baranchugov, E. Markevich, E. Pollak, G. Salitra, D. Aurbach, Amorphous silicon thin films as a high capacity anodes for Li-ion batteries in ionic liquid electrolytes, Electrochem. Commun. 9 (2007) 796–800.
[56] J.-K. Kim, G.-B. Cho, H.-S. Ryu, H.-J. Ahn, K.-K. Cho, K.-W. Kim, A. Matic, P. Jacobsson, J.-H. Ahn, Electrochemical properties of a full cell of lithium iron phosphate cathode using thin amorphous silicon anode, Solid State Ionics 268 (2014) 256–260.
[57] K.L. Lee, J.Y. Jung, S.W. Lee, H.S. Moon, J.W. Park, Electrochemical characteristics of a-Si thin film anode for Li-ion rechargeable batteries, J. Power Sources 129 (2004) 270–274.
[58] H.X. Deng, C.Y. Chung, M. Park, C.H. Park, S.K. Joo, Effect of substrate surface conditions on electrochemical performance of Si thin film anode, ECS Trans. 2 (2007) 105–112.
[59] M. Uehara, J. Suzuki, K. Tamura, K. Sekine, T. Takamura, Thick vacuum deposited silicon films suitable for the anode of Li-ion battery, J. Power Sources 146 (2005) 441–444.
[60] T. Zhang, H.P. Zhang, L.C. Yang, B. Wang, Y.P. Wu, T. Takamura, The structural evolution and lithiation behavior of vacuum-deposited Si film with high reversible capacity, Electrochim. Acta 53 (2008) 5660–5664.
[61] M.T. Demirkan, L. Trahey, T. Karabacak, Cycling performance of density modulated multilayer silicon thin film anodes in Li-ion batteries, J. Power Sources 273 (2015) 52–61.
[62] M. Wang, Z. Geng, Facile synthesis of multilayer-like Si thin film as high-performance anode materials for lithium-ion batteries, Appl. Phys. A 122 (2016) 528.
[63] G. Cho, J. Noh, H. Sung, S. Lee, Y. Im, H. Ahn, K. Kim, Patterned Si thin film electrodes for enhancing structural stability, Nanoscale Res. Lett. 7 (2012) 20.
[64] G.B. Cho, J.P. Noh, H.J. Sung, S.Y. Choi, S.H. Lee, H.J. Ahn, T.H. Nam, K.W. Kim, Improved electrochemical properties of patterned Si film electrodes, Microelectron. Eng. 89 (2012) 104–108.
[65] X. Xiao, P. Liu, M.W. Verbrugge, H. Haftbaradaran, H. Gao, Improved cycling stability of silicon thin film electrodes through patterning for high energy density lithium batteries, J. Power Sources 196 (2011) 1409–1416.
[66] G.B. Cho, J.K. Kim, S.H. Lee, G. Kim, J. Noh, K. Cho, K. Kim, T. Nam, H. Ahn, Facile fabrication of patterned Si film electrodes containing trench-structured Cu current collectors for thin-film batteries, Electrochim. Acta 224 (2017) 649–659.
[67] J.-S. Jeong, M.-R. Chae, H.-B. Park, Y.-M. Im, H.-J. Ahn, T.-H. Nam, K.-W. Kim, G.-B. Cho, Annealing effect on electrochemical properties of patterned Si film electrodes for thin-film batteries, Curr. Appl. Phys. (2017) 1–5.
[68] C. Yu, X. Li, T. Ma, J. Rong, R. Zhang, J. Shaffer, Y. An, Q. Liu, B. Wei, H. Jiang, Silicon thin films as anodes for high-performance lithium-ion batteries with effective stress relaxation, Adv. Energy Mater 2 (2012) 68–73.
[69] L. Baggetto, D. Danilov, P.H.L. Notten, Honeycomb-structured silicon: remarkable morphological changes induced by electrochemical (De)lithiation, Adv. Mater. 23 (2011) 1563–1566.
[70] X. Wang, L. Huang, Y. Zhang, F. Yin, Z. Bakenov, N. Umirov, M. Jin, G. Zhou, Novel silicon nanowire film on copper foil as high performance anode for lithium-ion batteries, Ionics 24 (2018) 373–378.
[71] S. Fujitani, H. Yagi, K. Sayama, T. Yoshida, K. Tarui, New a-Si alloy thin film anode with self organized micro columnar structure, Electrochem. Soc. (2003) 1.
[72] M. Ge, J. Rong, X. Fang, C. Zhou, Porous doped silicon nanowires for lithium ion battery anode with long cycle life, Nano Lett. 12 (2012) 2318–2323.
[73] R. Lin, S. Zhang, Z. Du, H. Fang, Y. Ren, X. Wu, Copper nanowires based current collector for light-weight and flexible composite silicon anode with high stability and specific capacity, RSC Adv. 5 (2015) 87090–87097.
[74] A. Mukanova, A. Nurpeissova, S.S. Kim, M. Myronov, Z. Bakenov, N-type doped silicon thin film on a porous Cu current collector as the negative electrode for Li-Ion batteries, ChemistryOpen 7 (2018) 92–96.
[75] F. Dogan, L.D. Sanjeewa, S.J. Hwu, J.T. Vaughey, Electrodeposited copper foams as substrates for thin film silicon electrodes, Solid State Ionics 288 (2015) 204–206.
[76] X.H. Huang, J.B. Wu, Y.Q. Cao, P. Zhang, Y. Lin, R.Q. Guo, Cobalt nanosheet arrays supported silicon film as anode materials for lithium ion batteries, Electrochim. Acta 203 (2016) 213–220.

[77] X. Chen, K. Gerasopoulos, J. Guo, A. Brown, C. Wang, R. Ghodssi, J.N. Culver, A patterned 3D silicon anode fabricated by electrodeposition on a virus-structured current collector, Adv. Funct. Mater. 21 (2011) 380–387.

[78] J.O. Song, H.T. Shim, D.J. Byun, J.K. Lee, A study on the effect of structure and P-doping of Si thin film as an anode for lithium rechargeable batteries, Adv. Nanomater. Process 124–126 (2007) 1063–1066.

[79] H.J. Ahn, Y.S. Kim, W.B. Kim, Y.E. Sung, T.Y. Seong, Formation and characterization of Cu-Si nanocomposite electrodes for rechargeable Li batteries, J. Power Sources 163 (2006) 211–214.

[80] B.D. Polat, O.L. Eryilmaz, O. Keles, A. Erdemir, K. Amine, Compositionally graded SiCu thin film anode by magnetron sputtering for lithium ion battery, Thin Solid Films 596 (2015) 190–197.

[81] C.M. Hwang, C.H. Lim, J.H. Yang, J.W. Park, Electrochemical properties of negative $SiMo_x$ electrodes deposited on a roughened substrate for rechargeable lithium batteries, J. Power Sources 194 (2009) 1061–1067.

[82] J.B. Kim, H.Y. Lee, K.S. Lee, S.H. Lim, S.M. Lee, Fe/Si multi-layer thin film anodes for lithium rechargeable thin film batteries, Electrochem. Commun. 5 (2003) 544–548.

[83] J.B. Kim, B.S. Jun, S.M. Lee, Improvement of capacity and cyclability of Fe/Si multilayer thin film anodes for lithium rechargeable batteries, Electrochim. Acta 50 (2005) 3390–3394.

[84] Q. Zhang, J. Liu, Z.Y. Wu, J.T. Li, L. Huang, S.G. Sun, 3D nanostructured multilayer Si/Al film with excellent cycle performance as anode material for lithium-ion battery, J. Alloy. Comp. 657 (2016) 559–564.

[85] H. Liu, M. Zhu, Z. Du, M.N. Obrovac, The electrochemistry of amorphous Si-B thin film electrodes in Li cells, J. Electrochem. Soc. 163 (2015) A192–A196.

[86] H. Li, H. Bai, Z. Tao, J. Chen, Si-Y multi-layer thin films as anode materials of high-capacity lithium-ion batteries, J. Power Sources 217 (2012) 102–107.

[87] S. Guo, H. Li, H. Bai, Z. Tao, J. Chen, Ti/Si/Ti sandwich-like thin film as the anode of lithium-ion batteries, J. Power Sources 248 (2014) 1141–1148.

[88] Z. Wen, F. Tian, Cu-doped silicon film as anode for lithium ion batteries prepared by ion-beam sputtering, Int. J. Electrochem. Sci. 8 (2013) 10129–10137.

[89] Y.H. Wang, Y. He, R.J. Xiao, H. Li, K.E. Aifantis, X.J. Huang, Investigation of crack patterns and cyclic performance of Ti-Si nanocomposite thin film anodes for lithium ion batteries, J. Power Sources 202 (2012) 236–245.

[90] V.A. Sethuraman, K. Kowolik, V. Srinivasan, Increased cycling efficiency and rate capability of copper-coated silicon anodes in lithium-ion batteries, J. Power Sources 196 (2011) 393–398.

[91] S. Hieu, N.J. Lim, Improving the performance of silicon anode in lithium-ion batteries by Cu2O coating layer, J. Appl. Electrochem. 44 (2014) 353–360.

[92] M.K. Datta, J. Maranchi, S.J. Chung, R. Epur, K. Kadakia, P. Jampani, P.N. Kumta, Amorphous silicon-carbon based nano-scale thin film anode materials for lithium ion batteries, Electrochim. Acta 56 (2011) 4717–4723.

[93] N. Garino, E. Biserni, A.L. Bassi, P. Bruno, C. Gerbaldi, Mesoporous Si and multi-layered Si/C films by pulsed laser deposition as Li-Ion microbattery anodes, J. Electrochem. Soc. 162 (2015) A1816–A1822.

[94] A.A. Arie, J.O. Song, J.K. Lee, Structural and electrochemical properties of fullerene-coated silicon thin film as anode materials for lithium secondary batteries, Mater. Chem. Phys. 113 (2009) 249–254.

[95] E. Biserni, M. Xie, R. Brescia, A. Scarpellini, M. Hashempour, P. Movahed, S.M. George, M. Bestetti, A. Li Bassi, P. Bruno, Silicon algae with carbon topping as thin-film anodes for lithium-ion microbatteries by a two-step facile method, J. Power Sources 274 (2015) 252–259.

[96] C. Wu, C. Chang, J. Duh, Silicon nitride coated silicon thin fi lm on three dimensions current collector for lithium ion battery anode, J. Power Sources 325 (2016) 64–70.

[97] M. Haro, V. Singh, S. Steinhauer, E. Toulkeridou, Nanoscale heterogeneity of multilayered Si anodes with embedded nanoparticle scaffolds for Li-Ion batteries, 1700180, Adv. Sci. (2017), 1700180.

[98] Y. Tong, Z. Xu, C. Liu, G. Zhang, J. Wang, Z.G. Wu, Magnetic sputtered amorphous Si/C multilayer thin films as anode materials for lithium ion batteries, J. Power Sources 247 (2014) 78–83.

[99] K. Xu, Y. He, L. Ben, H. Li, X. Huang, Enhanced electrochemical performance of Si-Cu-Ti thin films by surface covered with $Cu_3Si$ nanowires, J. Power Sources 281 (2015) 455–460.

[100] J. Brumbarov, J. Kunze-Liebhäuser, Silicon on conductive self-organized $TiO_2$ nanotubes – a high capacity anode material for Li-ion batteries, J. Power Sources 258 (2014) 129–133.

[101] J. Lin, J. Guo, C. Liu, H. Guo, Artificial solid electrolyte interphase with in-situ formed porosity for enhancing lithiation of silicon wafer, J. Power Sources 336 (2016) 401–407.

[102] W. Sun, R. Hu, H. Liu, M. Zeng, L. Yang, H. Wang, M. Zhu, Embedding nano-silicon in graphene nanosheets by plasma assisted milling for high capacity anode materials in lithium ion batteries, J. Power Sources 268 (2014) 610–618.

[103] U. Toçoğlu, G. Hatipoğlu, M. Alaf, F. Kayış, H. Akbulut, Electrochemical characterization of silicon/graphene/MWCNT hybrid lithium-ion battery anodes produced via RF magnetron sputtering, Appl. Surf. Sci. 389 (2016) 507–513.

[104] A. Mukanova, A. Nurpeissova, A. Urazbayev, S. Kim, M. Myronov, Z. Bakenov, Silicon thin film on graphene coated nickel foam as an anode for Li-ion batteries, Electrochim. Acta 258 (2017) 800–806.

[105] K.F. Chiu, S.H. Su, H.J. Leu, C.Y. Wu, Silicon thin film anodes coated on micron carbon-fiber current collectors for lithium ion batteries, Surf. Coating. Technol. 267 (2015) 70–74.

[106] Y.Q. Zhang, X.H. Xia, X.L. Wang, Y.J. Mai, S.J. Shi, Y.Y. Tang, L. Li, J.P. Tu, Silicon/graphene-sheet hybrid fi lm as anode for lithium ion batteries, Electrochem. Commun. 23 (2012) 17–20.

[107] G. Radhakrishnan, P.M. Adams, B. Foran, M.V. Quinzio, M.J. Brodie, Pulsed laser deposited Si on multilayer graphene as anode material for lithium ion batteries, Apl. Mater. 1 (2013) 62103.

[108] H. Sun, A.E.D.R. Castillo, S. Monaco, A. Capasso, A. Ansaldo, M. Prato, D.A. Dinh, V. Pellegrini, B. Scrosati, L. Manna, F. Bonaccorso, Binder-free graphene as advanced anode for lithium batteries Haiyan, J. Mater. Chem. A 4 (2016) 6886–6895.

[109] F.J. Sonia, M.K. Jangid, B. Ananthoju, M. Aslam, P. Johari, A. Mukhopadhyay, Understanding the Li-storage in few layers graphene with respect to bulk graphite: experimental, analytical and computational study, J. Mater. Chem. A Mater. Energy Sustain. 5 (2017) 8662–8679.

[110] T.M. Paronyan, A.K. Thapa, A. Sherehiy, J.B. Jasinski, J.S.D. Jangam, Incommensurate graphene foam as a high capacity lithium intercalation anode, Sci. Rep. 7 (2017) 39944.

[111] W. Sun, R. Hu, H. Liu, H. Zhang, J. Liu, L. Yang, H. Wang, M. Zhu, Silicon/Wolfram Carbide@Graphene composite: enhancing conductivity and structure stability in amorphous-silicon for high lithium storage performance, Electrochim. Acta 191 (2016) 462–472.

[112] R. Hu, W. Sun, Y. Chen, M. Zeng, M. Zhu, Silicon/graphene based nanocomposite anode: large-scale production and stable high capacity for lithium ion batteries, J. Mater. Chem. A 2 (2014) 9118–9125.

[113] J.S. Custer, M.O. Thompson, D.C. Jacobson, J.M. Poate, S. Roorda, W.C. Sinke, F. Spaepen, Density of amorphous Si, Appl. Phys. Lett. 64 (1994) 437–439.

[114] M. Choi, Y. Xiao, J. Hwang, I. Belharouak, Y. Sun, Novel strategy to improve the Li-storage performance of micro silicon anodes, J. Power Sources 348 (2017) 302–310.

[115] J. Liang, X. Li, Z. Hou, W. Zhang, Y. Zhu, Y. Qian, A deep reduction and partial oxidation strategy for fabrication of mesoporous Si anode for lithium ion batteries, ACS Nano 10 (2016) 2295–2304.

[116] C.K. Chan, R. Ruffo, S.S. Hong, Y. Cui, Surface chemistry and morphology of the solid electrolyte interphase on silicon nanowire lithium-ion battery anodes, J. Power Sources 189 (2009) 1132–1140.

[117] N.S. Choi, K.H. Yew, H. Kim, S.S. Kim, W.U. Choi, Surface layer formed on silicon thin-film electrode in lithium bis(oxalato) borate-based electrolyte, J. Power Sources 172 (2007) 404–409.

[118] N.S. Choi, K.H. Yew, K.Y. Lee, M. Sung, H. Kim, S.S. Kim, Effect of fluoroethylene carbonate additive on interfacial properties of silicon thin-film electrode, J. Power Sources 161 (2006) 1254–1259.

[119] K. Fridman, R. Sharabi, R. Elazari, G. Gershinsky, E. Markevich, G. Salitra, D. Aurbach, A. Garsuch, J. Lampert, A new advanced lithium ion battery: combination of high performance amorphous columnar silicon thin film anode, 5 V $LiNi_{0.5}Mn_{15}O_4$ spinel cathode and fluoroethylene carbonate-based electrolyte solution, Electrochem. Commun. 33 (2013) 31–34.

[120] L. Chen, K. Wang, X. Xie, J. Xie, Enhancing electrochemical performance of silicon film anode by vinylene carbonate electrolyte additive, Electrochem. Solid State Lett. 9 (2006) A512–A515.

[121] T.L. Kulova, Irreversible capacity of the amorphous silicon thin-film electrodes, Russ. J. Electrochem. 44 (2008) 525–529.

[122] S.-W. Song, S.-W. Baek, Silane-derived SEI stabilization on thin-film electrodes of nanocrystalline Si for lithium batteries, Electrochem. Solid State Lett. 12 (2009) A23–A27.

[123] Y.-G. Ryu, S. Lee, S. Mah, D.J. Lee, K. Kwon, S. Hwang, S. Doo, Electrochemical behaviors of silicon electrode in lithium salt solution containing alkoxy silane additives, J. Electrochem. Soc. 155 (2008) A583–A589.

[124] X. Teng, C. Zhan, Y. Bai, L. Ma, Q. Liu, C. Wu, F. Wu, Y. Yang, J. Lu, K. Amine, In-situ analysis of gas generation in lithium ion batteries with different carbonate-based electrolytes, ACS Appl. Mater. Interfaces 7 (2015) 22751–22755.

[125] M. Winter, P. Novak, Chloroethylene carbonate, a solvent for lithium-ion cells, evolving CO2 during reduction, J. Electrochem. Soc. 145 (1998) L27–L30.

[126] A. Schiele, B. Breitung, T. Hatsukade, B.B. Berkes, P. Hartmann, J. Janek, T. Brezesinski, The critical role of fluoroethylene carbonate in the gassing of silicon anodes for lithium-ion batteries, ACS Energy Lett. 2 (2017) 2228–2233.

[127] M.E. Spahr, T. Palladino, H. Wilhelm, A. Würsig, D. Goers, H. Buqa, M. Holzapfel, P. Novak, Exfoliation of graphite during electrochemical lithium insertion in ethylene carbonate-containing electrolytes, J. Electrochem. Soc. 151 (2004) A1383–A1395.

[128] K. Hancock, J. Becherer, M. Hagen, M. Joos, M. Abert, D. Müller, P. Fanz, S. Straach, J. Tübke, Electrolyte decomposition and electrode thickness changes in Li-S cells with lithium metal anodes, prelithiated silicon anodes and hard carbon anodes, J. Electrochem. Soc. 165 (2018) A6091–A6106.

[129] K. Takada, Progress and prospective of solid-state lithium batteries, Acta Mater. 61 (2013) 759–770.

[130] S. Ohta, T. Kobayashi, J. Seki, T. Asaoka, Electrochemical performance of an all-solid-state lithium ion battery with garnet-type oxide electrolyte, J. Power Sources 202 (2012) 332–335.

[131] J.W. Fergus, Ceramic and polymeric solid electrolytes for lithium-ion batteries, J. Power Sources 195 (2010) 4554–4569.

[132] M.S. Whittingham, Lithium batteries and cathode materials, Chem. Rev. 104 (2004) 4271–4301.

[133] R. Miyazaki, N. Ohta, T. Ohnishi, K. Takada, Anode properties of silicon-rich amorphous silicon suboxide fi lms in all-solid-state lithium batteries, J. Power Sources 329 (2016) 41–49.
[134] J.F.M. Oudenhoven, L. Baggetto, P.H.L. Notten, All-solid-state lithium-ion microbatteries: a review of various three-dimensional concepts, Adv. Energy Mater. 1 (2011) 10–33.
[135] L. Baggetto, R.A.H. Niessen, F. Roozehoom, P.H.L. Notten, High energy density all-solid-state batteries: a challenging concept towards 3D integration, Adv. Funct. Mater. 18 (2008) 1057–1066.
[136] F. Le Cras, B. Pecquenard, V. Dubois, V.P. Phan, D. Guy-Bouyssou, All-solid-state lithium-ion microbatteries using silicon nanofilm anodes: high performance and memory effect, Adv. Energy Mater 5 (2015) 1501061.
[137] V.P. Phan, B. Pecquenard, F. Le Cras, High-performance all-solid-state cells fabricated with silicon electrodes, Adv. Funct. Mater. 22 (2012) 2580–2584.
[138] C. Gong, D. Ruzmetov, A. Pearse, D. Ma, J.N. Munday, G. Rubloff, A.A. Talin, M.S. Leite, Surface/interface effects on high-performance thin-film all-solid-state Li-Ion batteries, ACS Appl. Mater. Interfaces 7 (2015) 26007–26011.
[139] A.A. Talin, D. Ruzmetov, A. Kolmakov, K. McKelvey, N. Ware, F. El Gabaly, B. Dunn, H.S. White, Fabrication, testing, and simulation of all-solid-state three-dimensional Li-Ion batteries, ACS Appl. Mater. Interfaces 8 (2016) 32385–32391.
[140] N. Kamaya, K. Homma, Y. Yamakawa, M. Hirayama, R. Kanno, M. Yonemura, T. Kamiyama, Y. Kato, S. Hama, K. Kawamoto, A. Mitsui, A lithium superionic conductor, Nat. Mater. 10 (2011) 682–686.
[141] J. Tan, A. Tiwari, Fabrication and characterization of Li7La3Zr2O12 thin films for lithium ion battery, ECS Solid State Lett. 1 (2012) Q57–Q60.
[142] R.-J. Chen, M. Huang, W.-Z. Huang, Y. Shen, Y.-H. Lin, C.-W. Nan, Sol–gel derived Li–La–Zr–O thin films as solid electrolytes for lithium-ion batteries, J. Mater. Chem. A 2 (2014) 13277–13282.
[143] C.H. Choi, W.I. Cho, B.W. Cho, H.S. Kim, Y.S. Yoon, Y.S. Tak, Radio-frequency magnetron sputtering power effect on the ionic conductivities of lipon films, Electrochem. Solid State Lett. 5 (2002) A14–A17.
[144] S. Lobe, C. Dellen, M. Finsterbusch, H.-G. Gehrke, D. Sebold, C.-L. Tsai, S. Uhlenbruck, O. Guillon, Radio frequency magnetron sputtering of $Li_7La_3Zr_2O_{12}$ thin films for solid-state batteries, J. Power Sources 307 (2016) 684–689.
[145] S.H. Jee, M.J. Lee, H.S. Ahn, D.J. Kim, J.W. Choi, S.J. Yoon, S.C. Nam, S.H. Kim, Y.S. Yoon, Characteristics of a new type of solid-state electrolyte with a LiPON interlayer for Li-ion thin film batteries, Solid State Ionics 181 (2010) 902–906.
[146] Y. Hamon, A. Douard, F. Sabary, C. Marcel, P. Vinatier, B. Pecquenard, A. Levasseur, Influence of sputtering conditions on ionic conductivity of LiPON thin films, Solid State Ionics 177 (2006) 257–261.
[147] W.R. Torres, E. Herrera, A.Y. Tesio, E.J. Calvo, In situ generation of mesostructured $Cu_2S$/C composite cathode via electrochemical reaction for enhanced lithium storage and insights into the mechanism, ChemElectroChem 1 (2014) 375–378.
[148] S. Kim, M. Hirayama, S. Taminato, R. Kanno, Epitaxial growth and lithium ion conductivity of lithium-oxide garnet for an all solid-state battery electrolyte, Dalt. Trans. 42 (2013) 13112–13117.
[149] S. Swann, Magnetron sputtering, Phys. Technol. 19 (1988) 67–75.
[150] Ion Beam Sputter Deposition, Polygon Physics, 2016.
[151] D. Bäuerle, R. Rössler, J. Pedarnig, S.H. Yun, R. Dinu, N. Arnold, Pulsed laser deposition, Appl. Phys. A Mater. Sci. Process 69 (1999) S45–S48.
[152] W. Schwarzacher, Electrodeposition: a technology for the future, Electrochem. Soc. Interface 15 (2006) 32–35.
[153] R. Epur, M. Ramanathan, F.R. Beck, A. Manivannan, P.N. Kumta, Electrodeposition of amorphous silicon anode for lithium ion batteries, Mater. Sci. Eng. B 177 (2012) 1157–1162.
[154] B. Gattu, R. Epur, P.M. Shanti, P.H. Jampani, Pulsed current electrodeposition of silicon thin films anodes for lithiums ion battery applications, Inorg. Artic. 5 (2017) 1–14.
[155] C.A. Vlaic, S. Ivanov, R. Peipmann, A. Eisenhardt, M. Himmerlich, S. Krischok, A. Bund, Electrochemical lithiation of thin silicon based layers potentiostatically deposited from ionic liquid, Electrochim. Acta 168 (2015) 403–413.
[156] A. Mukanova, R. Tussupbayev, A. Sabitov, I. Bondarenko, R. Nemkaeva, B. Aldamzharov, Z. Bakenov, CVD graphene growth on a surface of liquida gallium, Mater. Today Proc. 4 (2017) 4548–4554.
[157] G. Colston, S.D. Rhead, V.A. Shah, O.J. Newell, I.P. Dolbnya, D.R. Leadley, M. Myronov, Mapping the strain state of 3C-SiC/Si (001) suspended structures using, Mater. Sci. Forum 858 (2016) 274–277.
[158] G. Ferraresi, L. Czornomaz, C. Villevieille, P. Novak, M. El Kazzi, Elucidating the surface reactions of an amorphous Si thin film as a model electrode for Li-Ion batteries, ACS Appl. Mater. Interfaces 8 (2016) 29791–29798.
[159] C. Pereira-Nabais, J. Światowska, A. Chagnes, F. Ozanam, A. Gohier, P. Tran-Van, C.S. Cojocaru, M. Cassir, P. Marcus, Interphase chemistry of Si electrodes used as anodes in Li-ion batteries, Appl. Surf. Sci. 266 (2013) 5–16.
[160] O.M. Vovk, B.K. Na, B.W. Cho, J.K. Lee, Electrochemical characteristics of amophous carbon coated silicon electrodes, Korean J. Chem. Eng. 26 (2009) 1034–1039.